ASTROFISICA

A.Giuliani - INAF / IASF Milano

giuliani@iasf-milano.inaf.it

www.iasf-milano.inaf.it/~giuliani/astrofisica2020

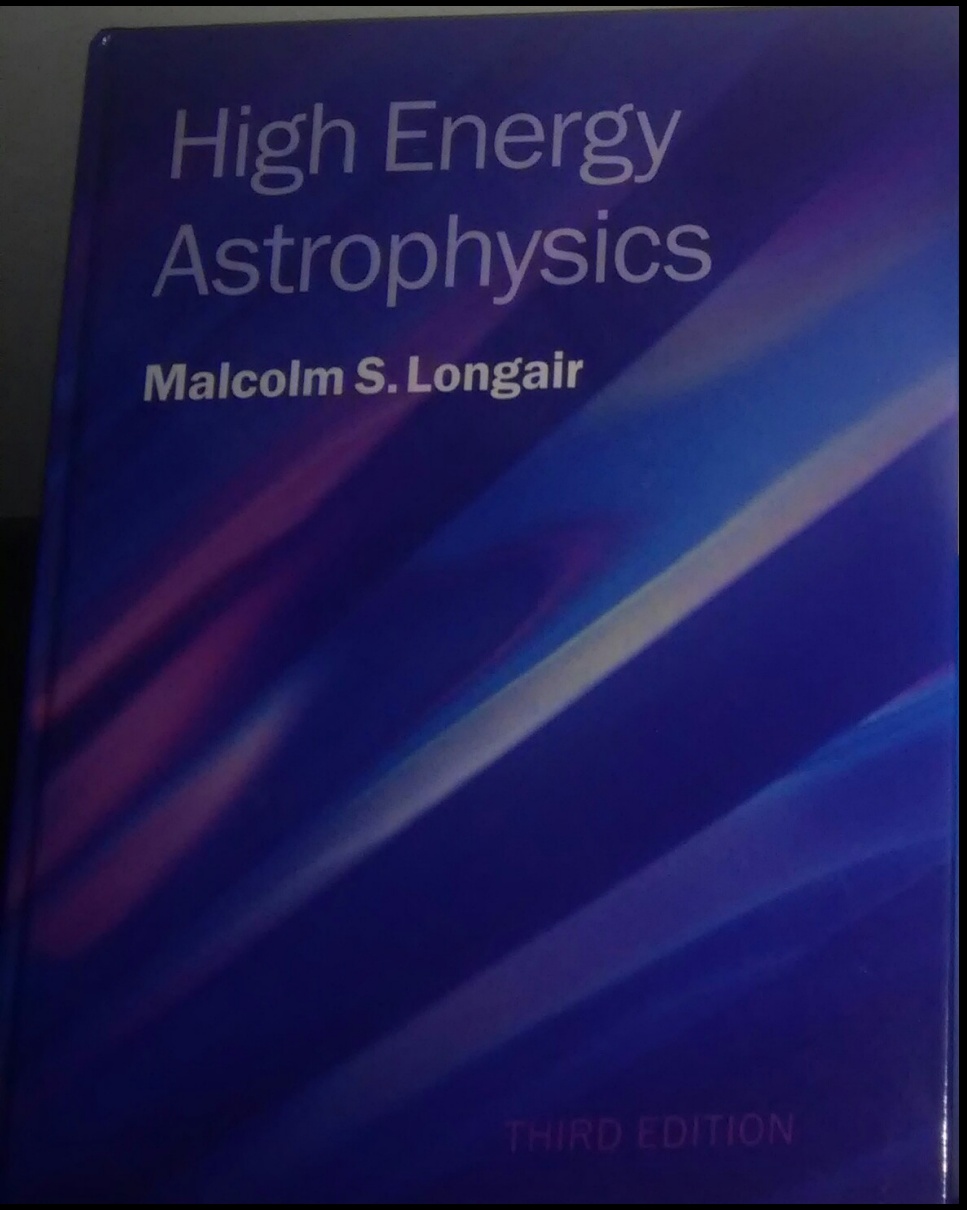

I take this term to mean the astrophysics of high energy processes and their application in astrophysical and cosmological contexts. These processes, their application in astrophysics and how they lead to some of the most challenging problems of contemporary physics, are the subjects of this book.

For example, we need to explain how the massive black holes present in the nuclei of active galaxies can be studied, how charged particles are accelerated to extremely high energies in astronomical environments, the origins of enormous fluxes of high energy particles and magnetic fields in active galaxies, the physical processes in the interiors and environments of neutron stars, the nature of the dark matter, the expected fluxes of gravitational waves in extreme astronomical environments, and so on.

Thus, high energy astrophysics makes feasible the study of the properties of matter under physical conditions which cannot yet be reproduced in the laboratory. Indeed, in many cases, the problems can only be addressed in the astrophysical environment.

The Milky Way Galaxy

Parallax

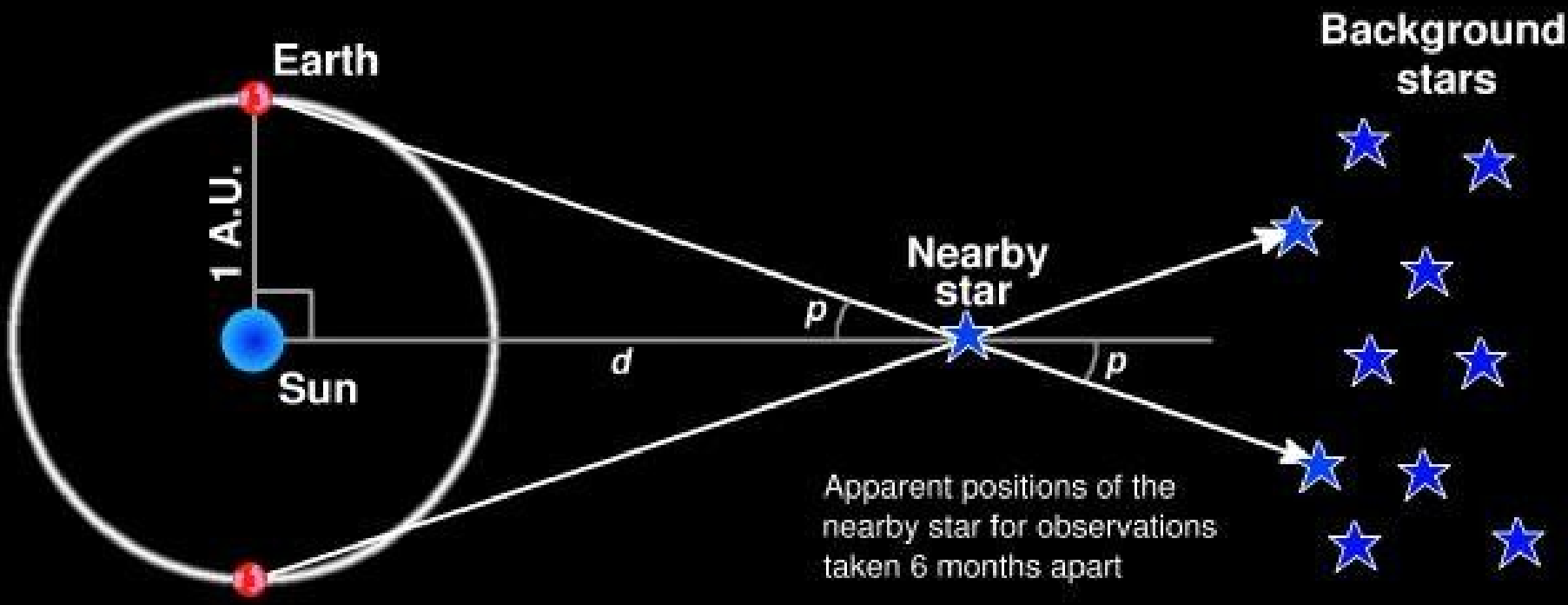
Earth
1 A.U.
Sun
d
p
Nearby star
p
Background stars
Apparent positions of the nearby star for observations taken 6 months apart

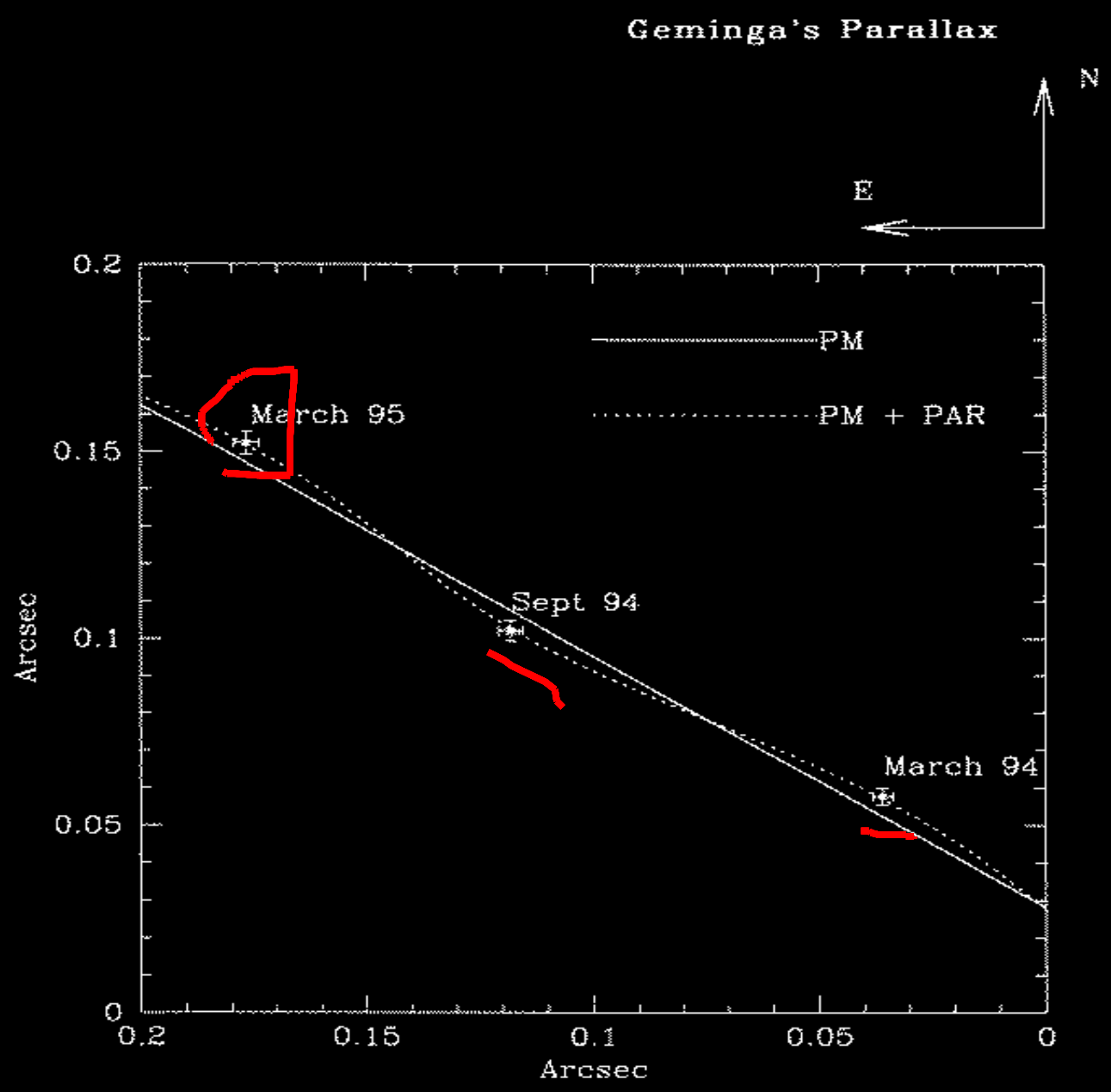
Geminga's Parallax
N
E
PM
PM + PAR
March 95
Sept 94
March 94
0.2
0.15
0.1
0.05
0
Arcsec
0.2
0.15
0.1
0.05
0
Arcsec

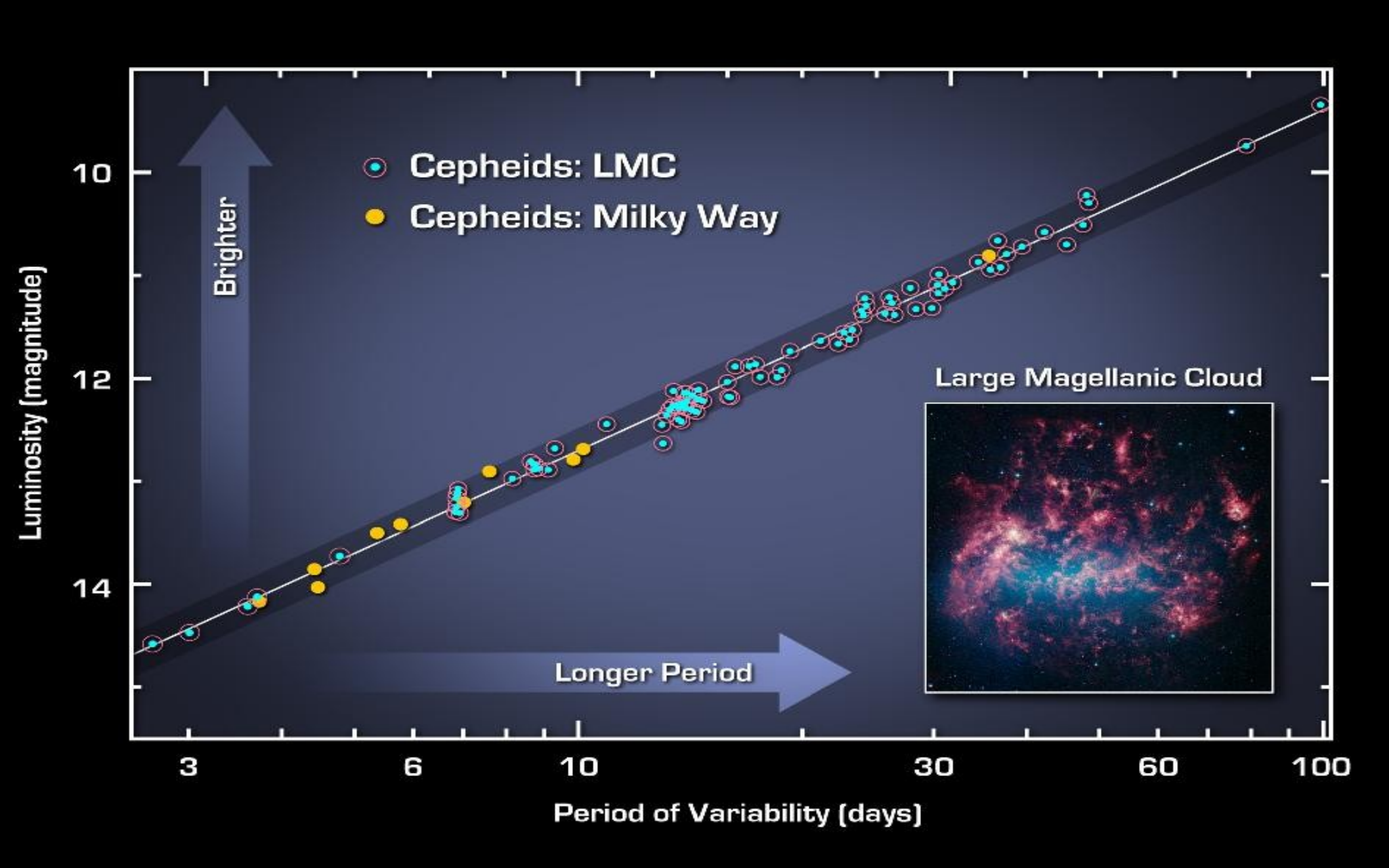
Cepheids: LMC
Cepheids: Milky Way
Brighter
Longer Period
Large Magellanic Cloud
Luminosity (magnitude)
10
12
14
3
6
10
30
60
100
Period of Variability (days)

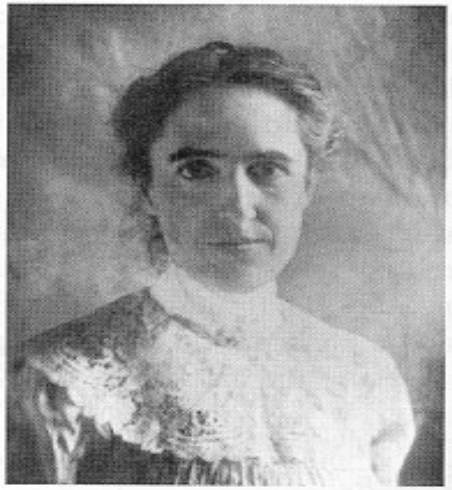

Figure 14.2 Henrietta Swan Leavitt (1868–1921). (Courtesy of Harvard College Observatory.)

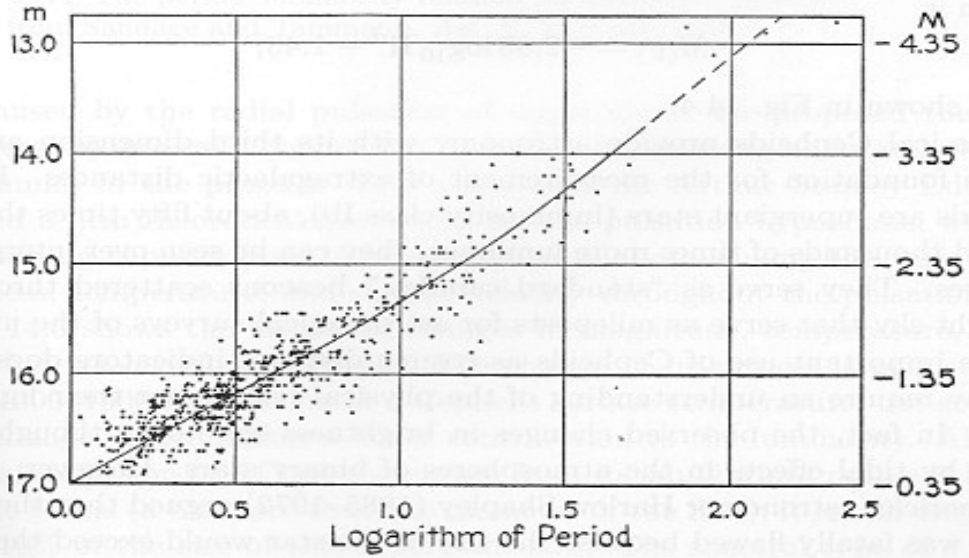

Figure 14.3 Classical Cepheids in the Small Magellanic Cloud, with the period in units of days. (Figure from Shapley, *Galaxies*, Harvard University Press, Cambridge, MA, 1961.)

Herschel's Galaxy

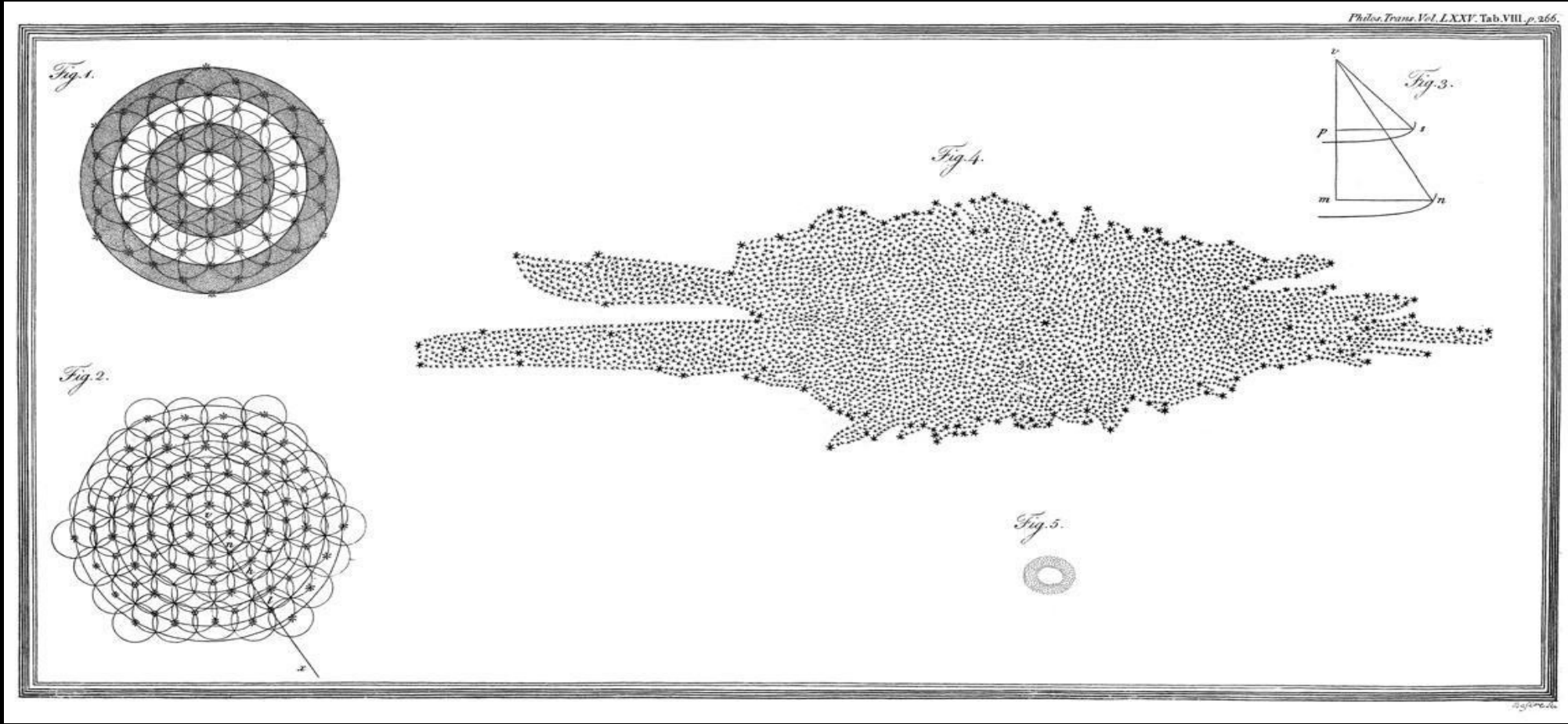

Globular Clusters

Shapley's Globular Cluster Distribution

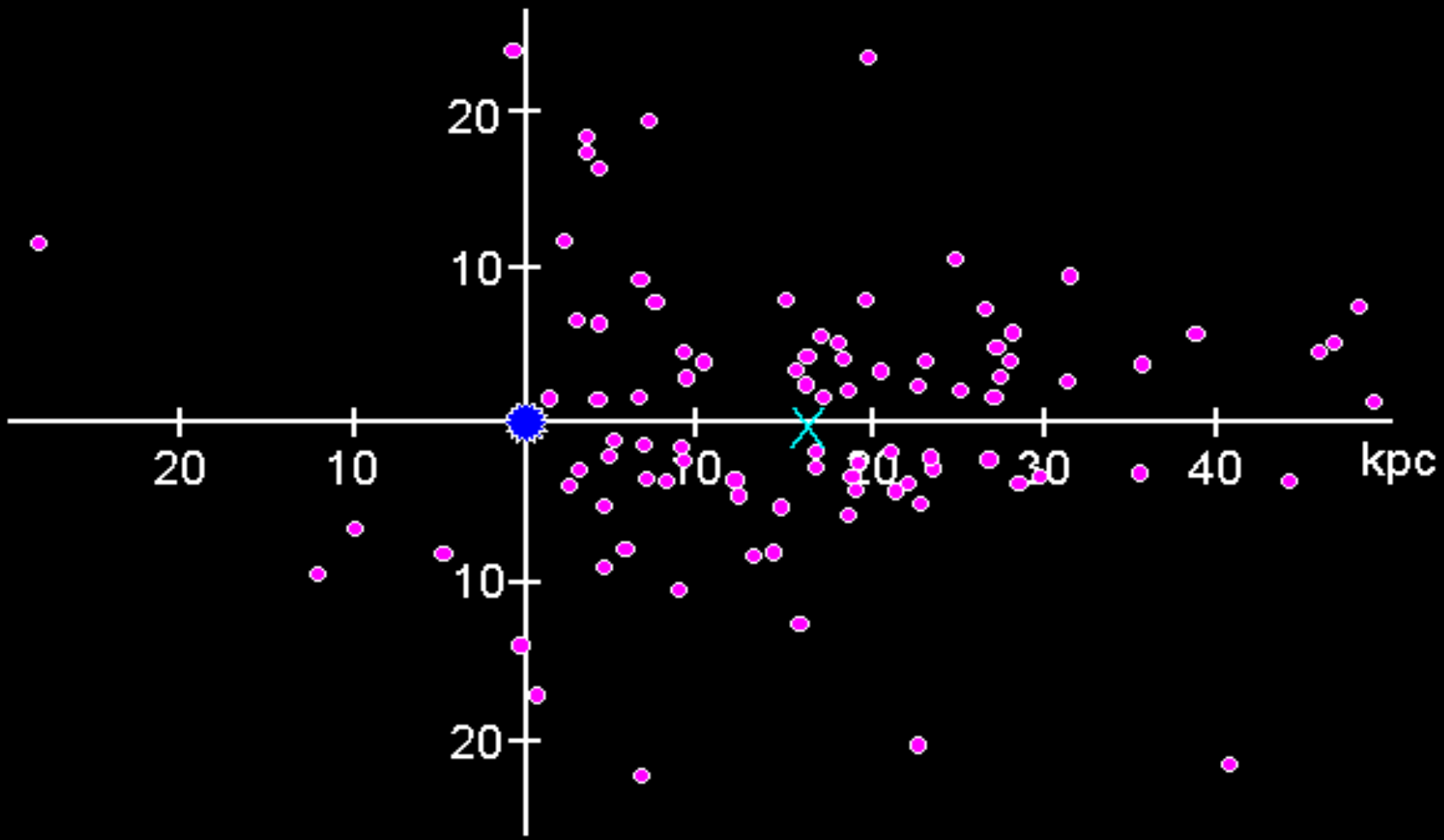

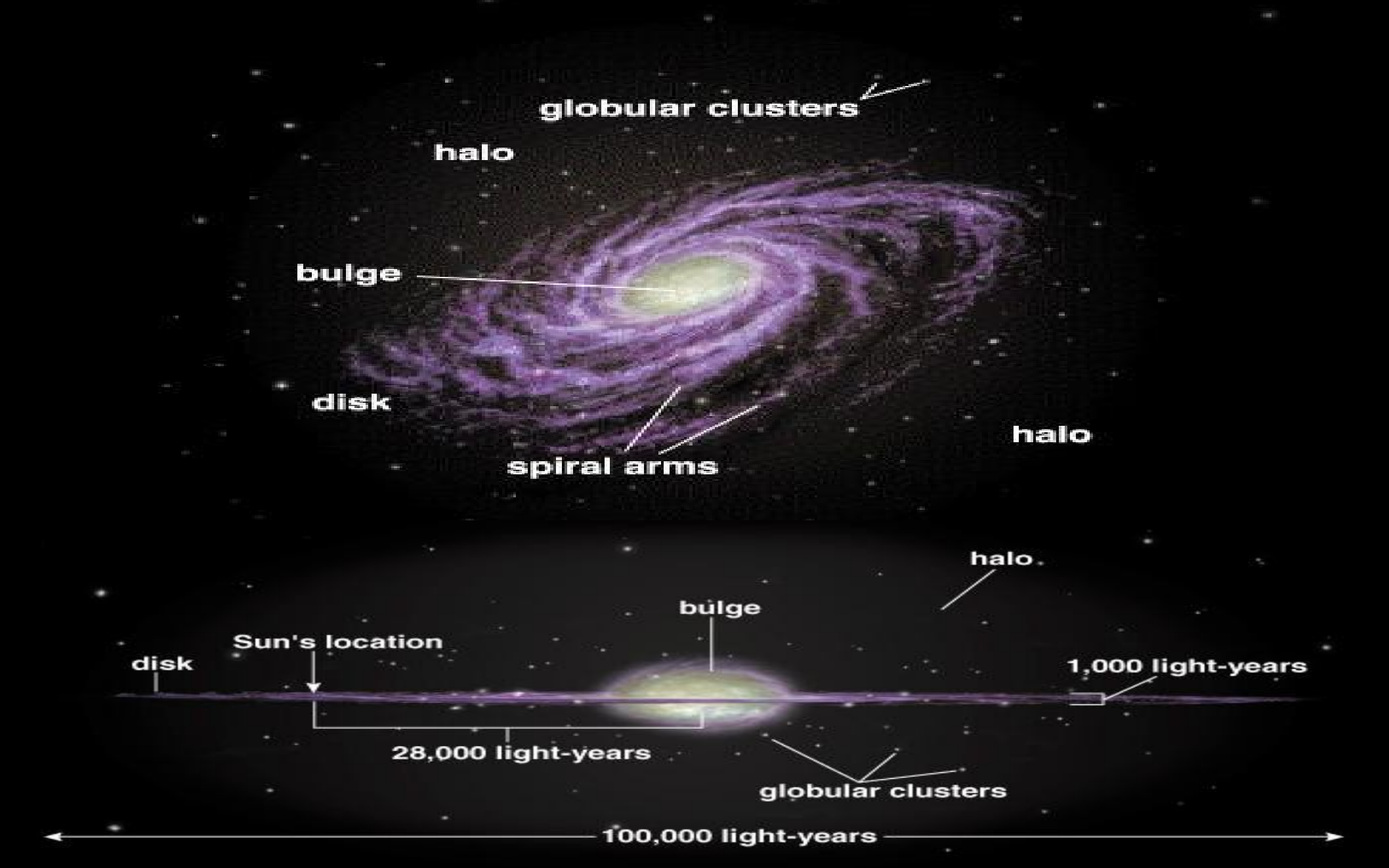
globular clusters
halo
bulge
disk
spiral arms
halo
halo
bulge
Sun's location
disk
1,000 light-years
28,000 light-years
globular clusters
100,000 light-years

The MilkyWay galaxy

A large SBb (or SBc) spiral galaxy with ongoing star formation

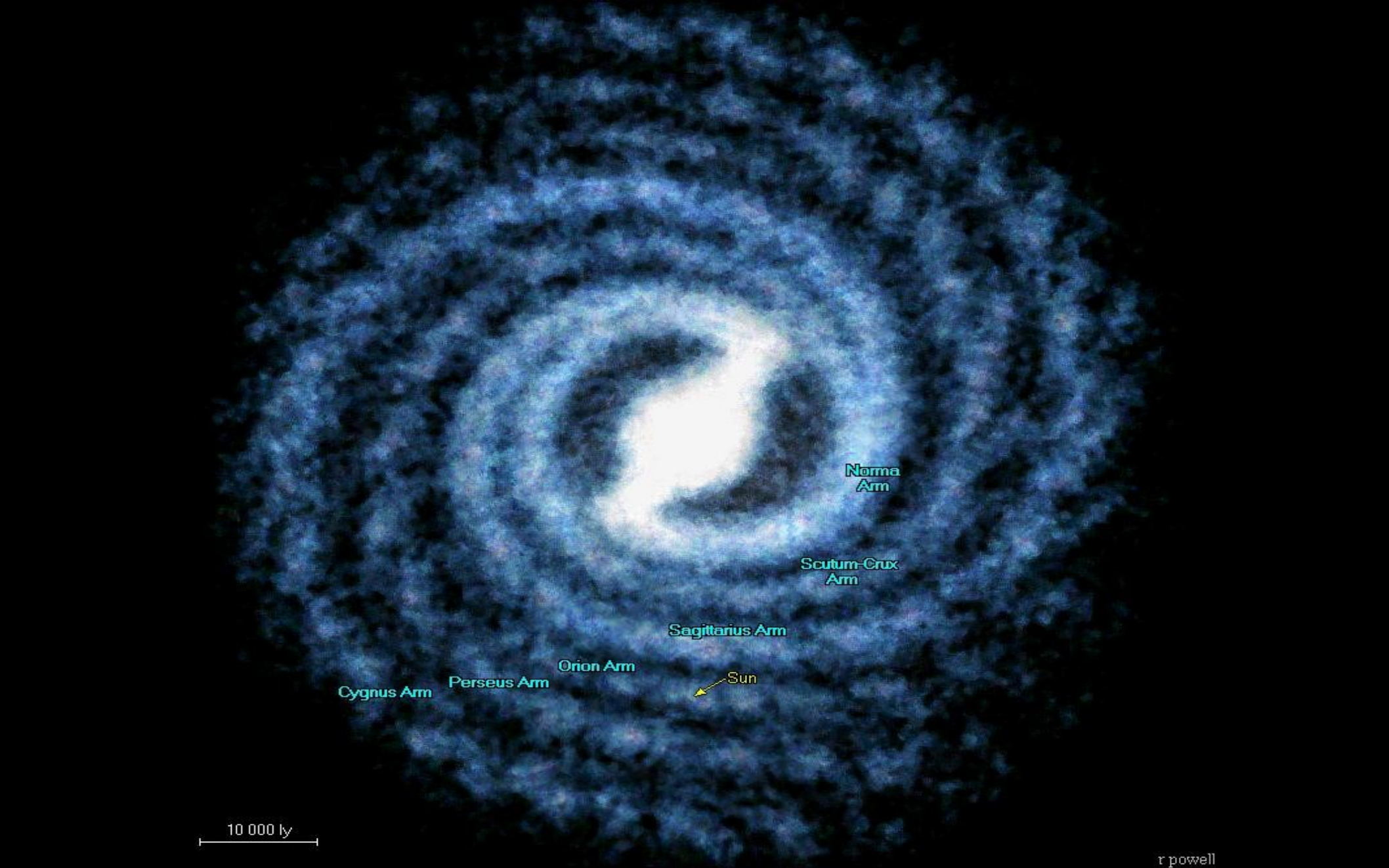
Norma Arm
Scutum-Crux Arm
Sagittarius Arm
Orion Arm
Sun
Perseus Arm
Cygnus Arm
10 000 ly
r powell

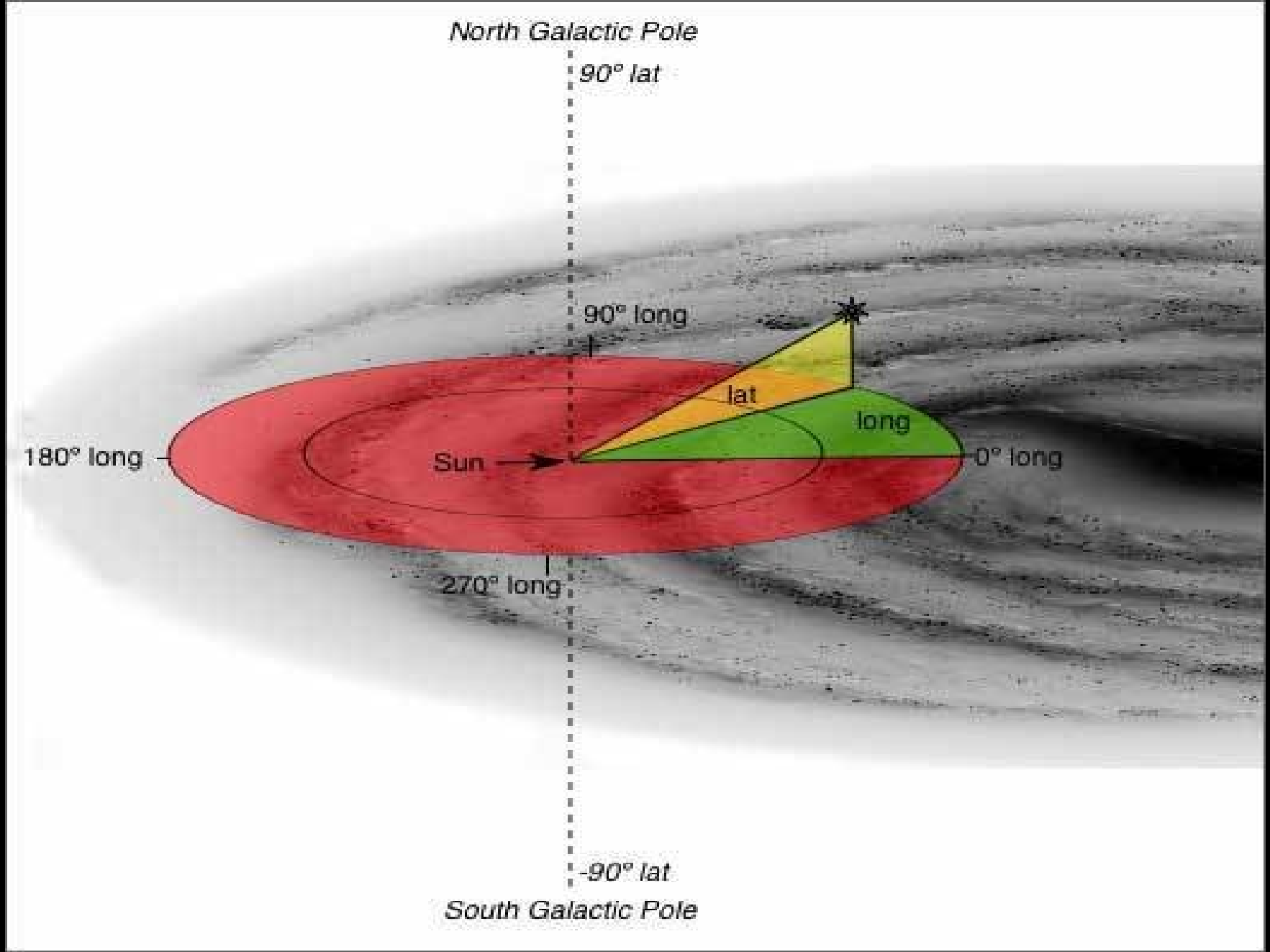
North Galactic Pole
90° lat
90° long
lat
long
180° long
Sun
0° long
270° long
-90° lat
South Galactic Pole

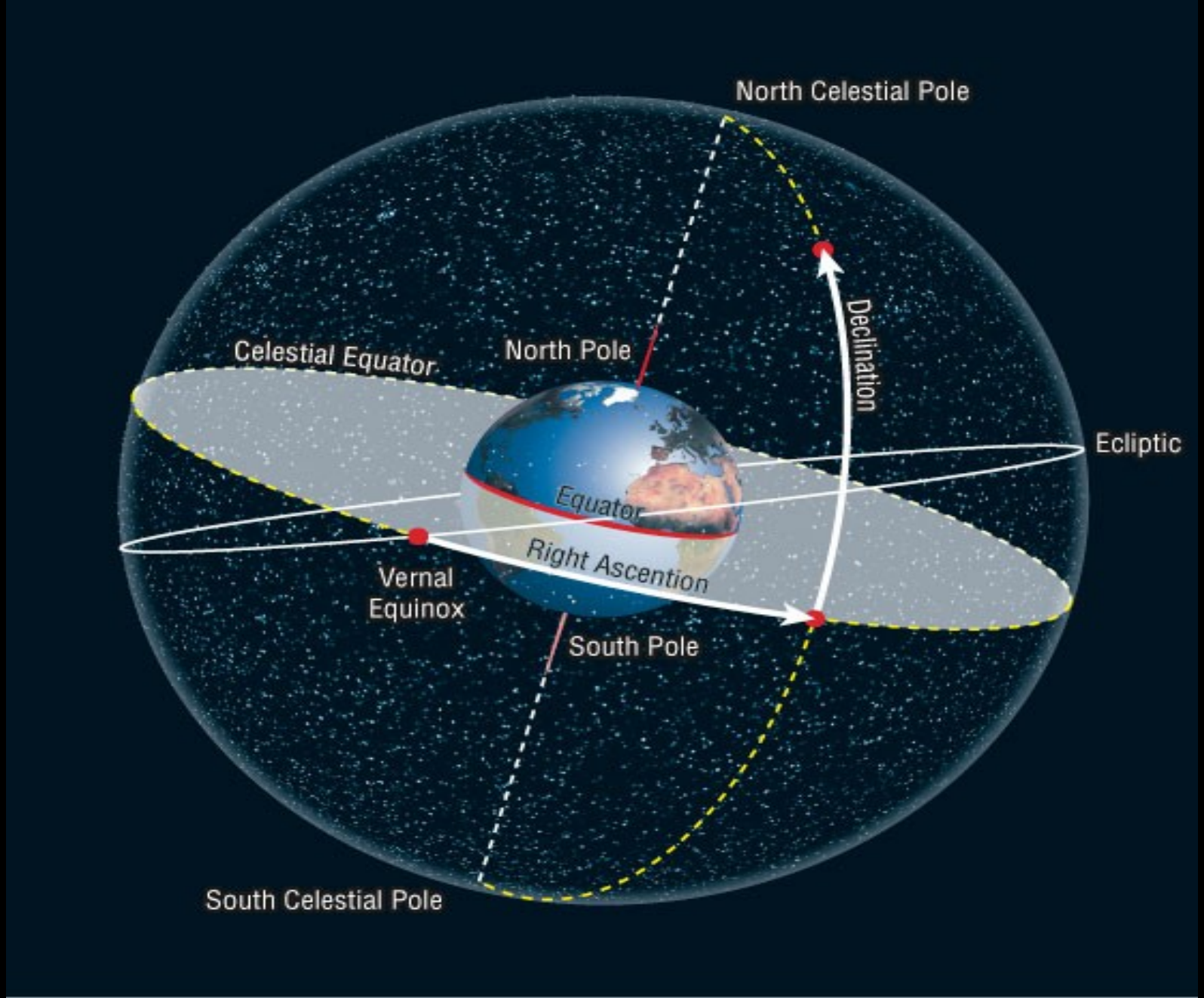
North Celestial Pole
Declination
Celestial Equator
North Pole
Ecliptic
Equator
Right Ascention
Vernal
Equinox
South Pole
South Celestial Pole

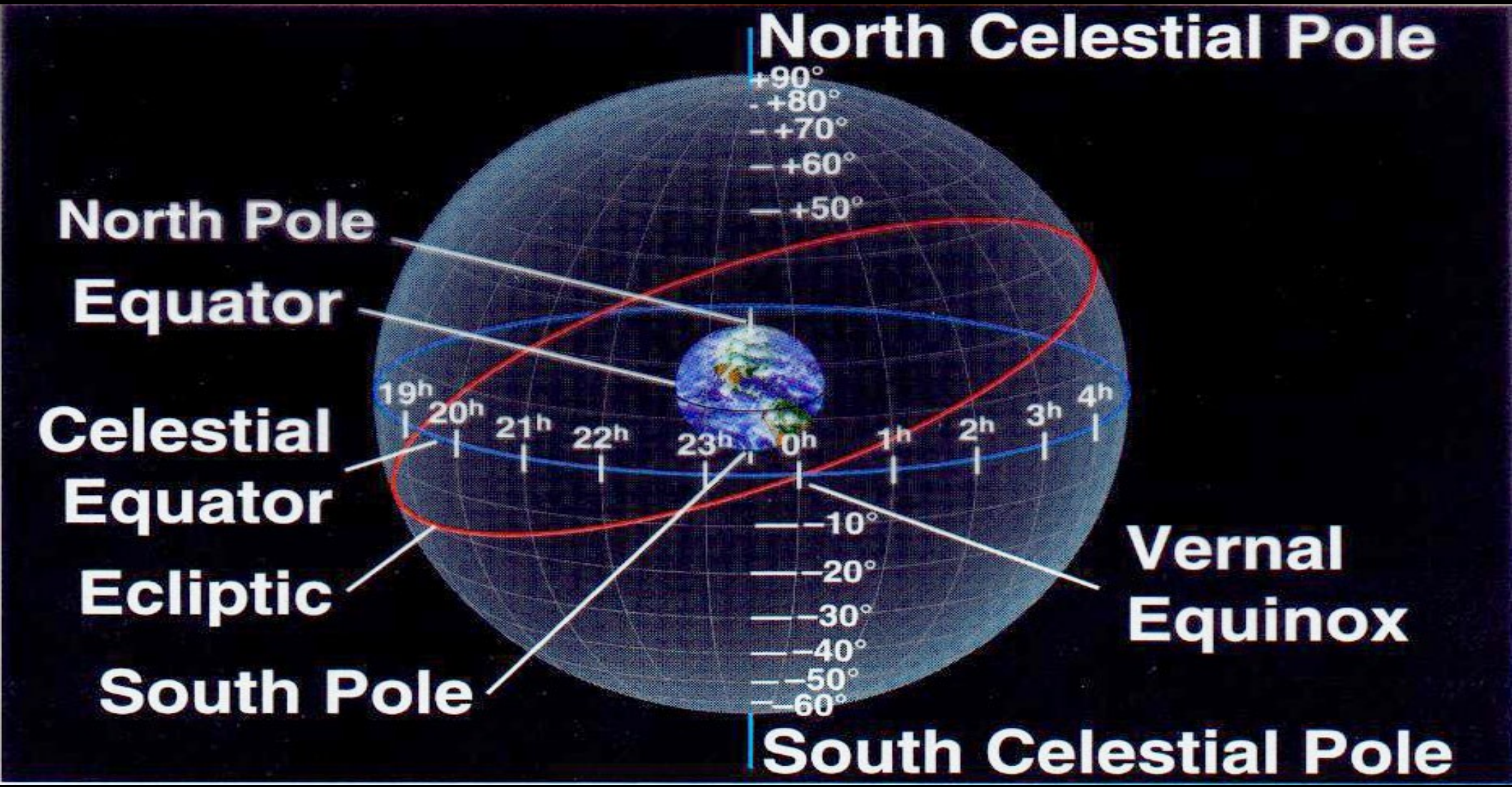
North Celestial Pole
+90°
+80°
+70°
+60°
+50°
North Pole
Equator
19h
20h
21h
22h
23h
0h
1h
2h
3h
4h
Celestial
Equator
Ecliptic
South Pole
−10°
−20°
−30°
−40°
−50°
−60°
Vernal
Equinox
South Celestial Pole

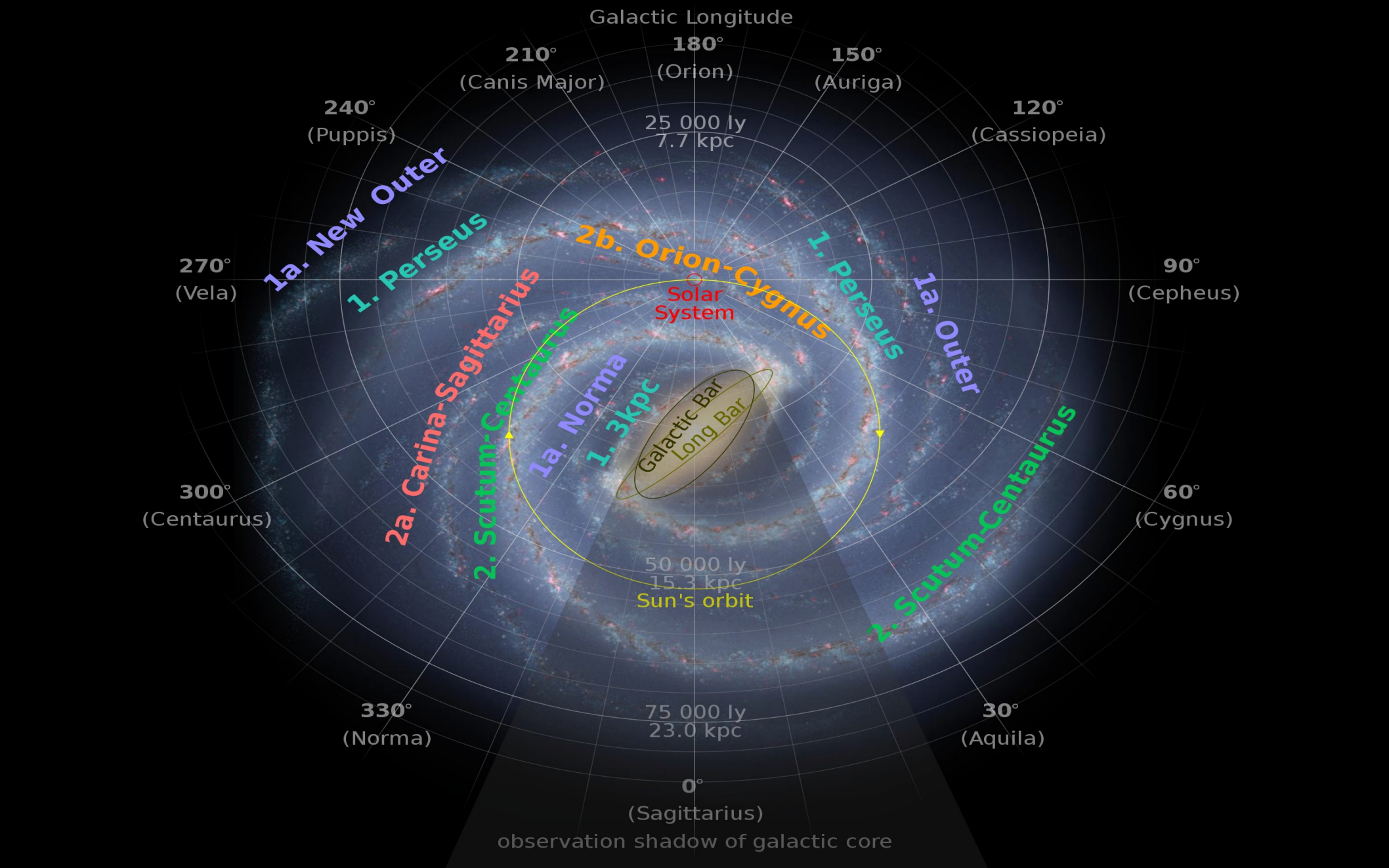
Galactic Longitude
180°
(Orion)
210°
(Canis Major)
150°
(Auriga)
240°
(Puppis)
120°
(Cassiopeia)
270°
(Vela)
90°
(Cepheus)
300°
(Centaurus)
60°
(Cygnus)
330°
(Norma)
30°
(Aquila)
0°
(Sagittarius)
25 000 ly
7.7 kpc
50 000 ly
15.3 kpc
75 000 ly
23.0 kpc
Solar System
Sun's orbit
Galactic Bar
Long Bar
1a. New Outer
1. Perseus
2b. Orion-Cygnus
1. Perseus
1a. Outer
2a. Carina-Sagittarius
2. Scutum-Centaurus
1a. Norma
1.3kpc
2. Scutum-Centaurus
observation shadow of galactic core

LOCAL GALACTIC GROUP

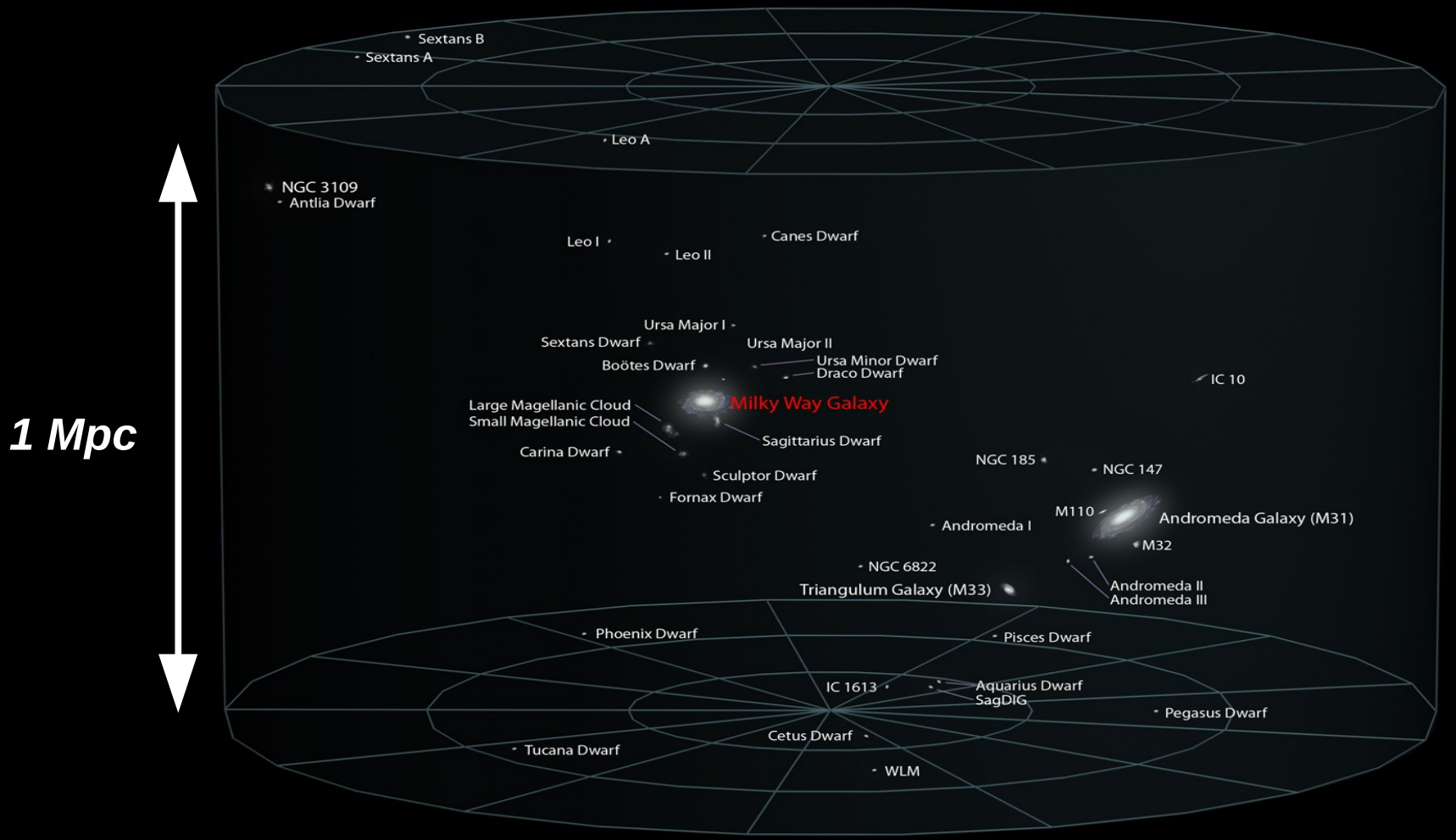

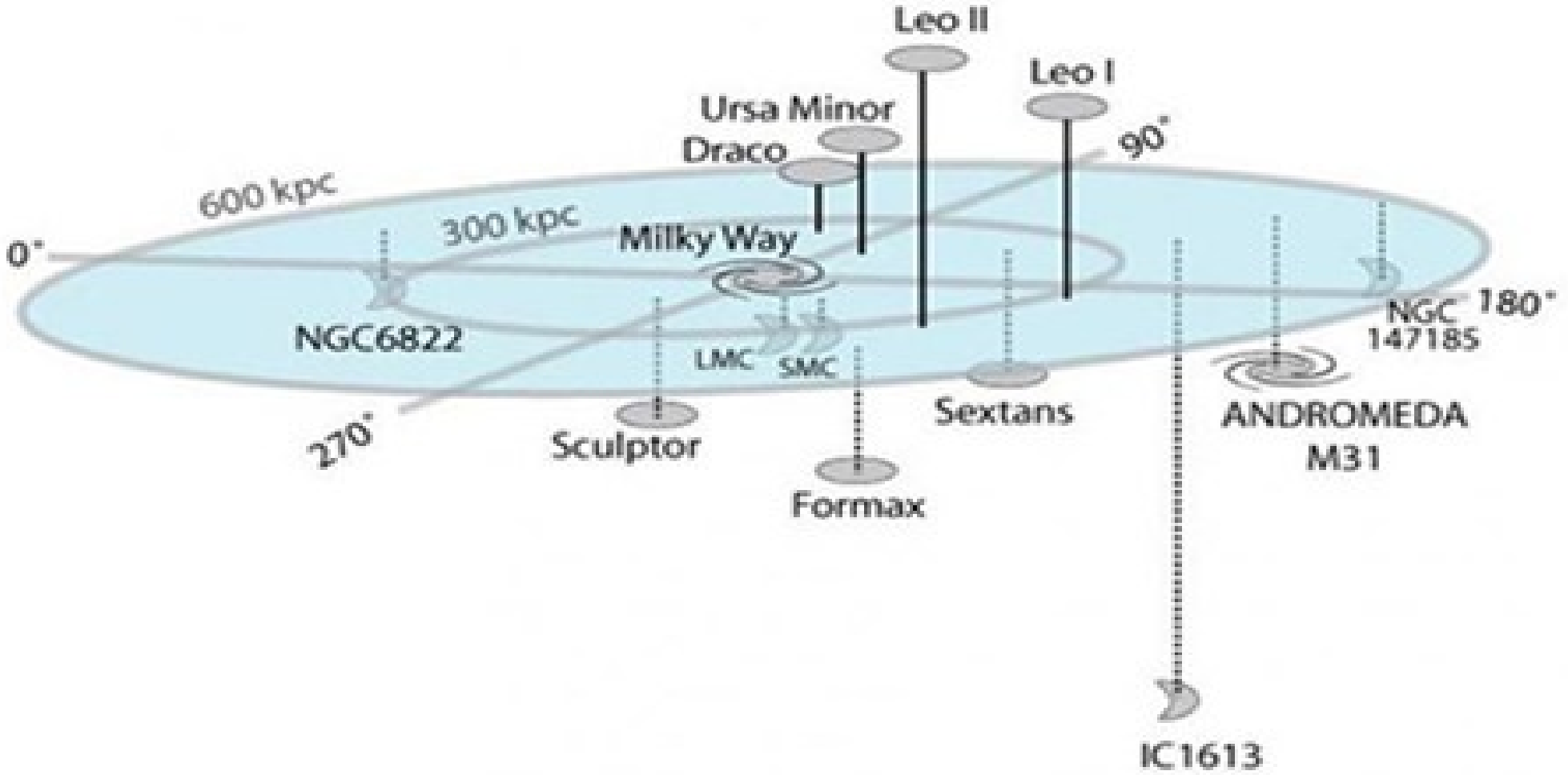
Leo II
Leo I
Ursa Minor
Draco
90°
600 kpc
300 kpc
0°
Milky Way
NGC6822
LMC
SMC
NGC 180°
147185
Sextans
ANDROMEDA
M31
270°
Sculptor
Formax
IC1613

Sagittarius Stream

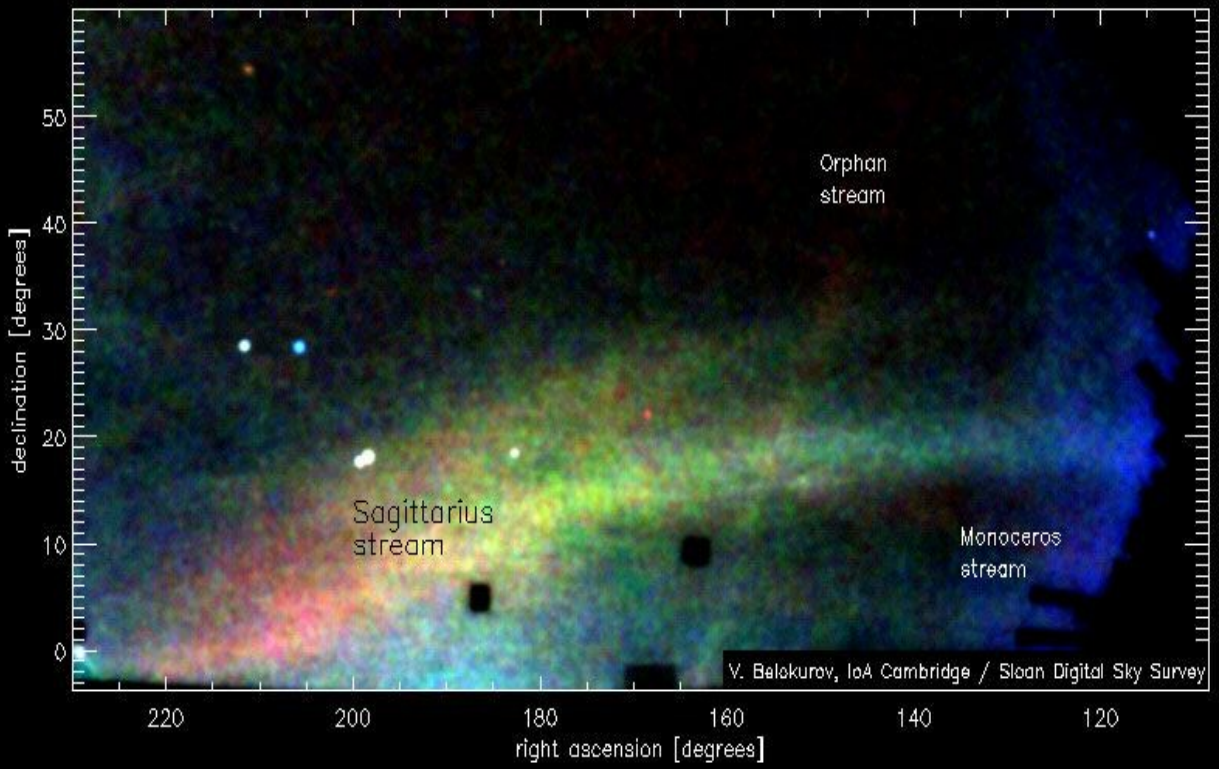

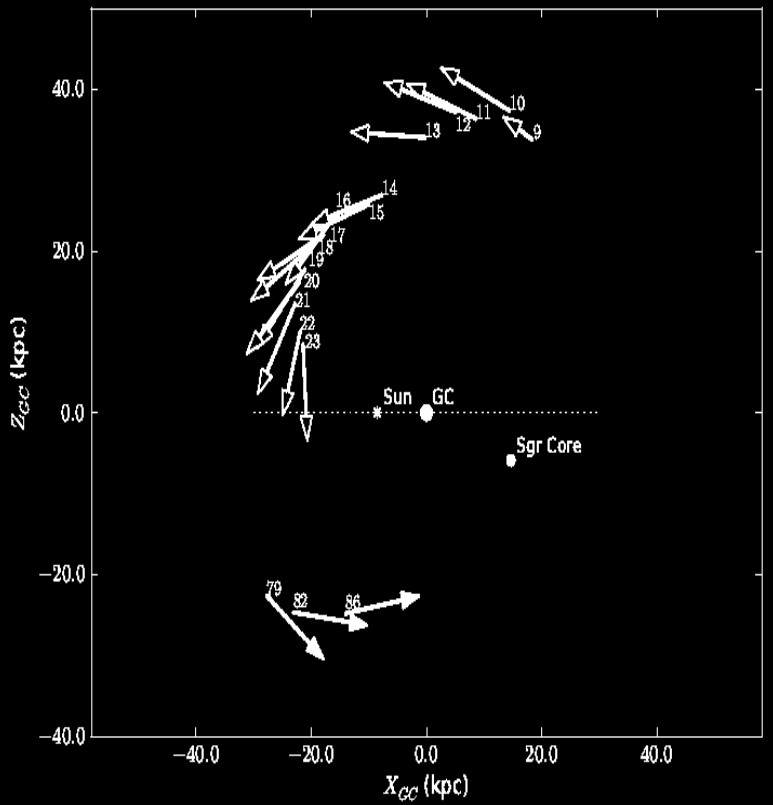

Sagittarius Stream

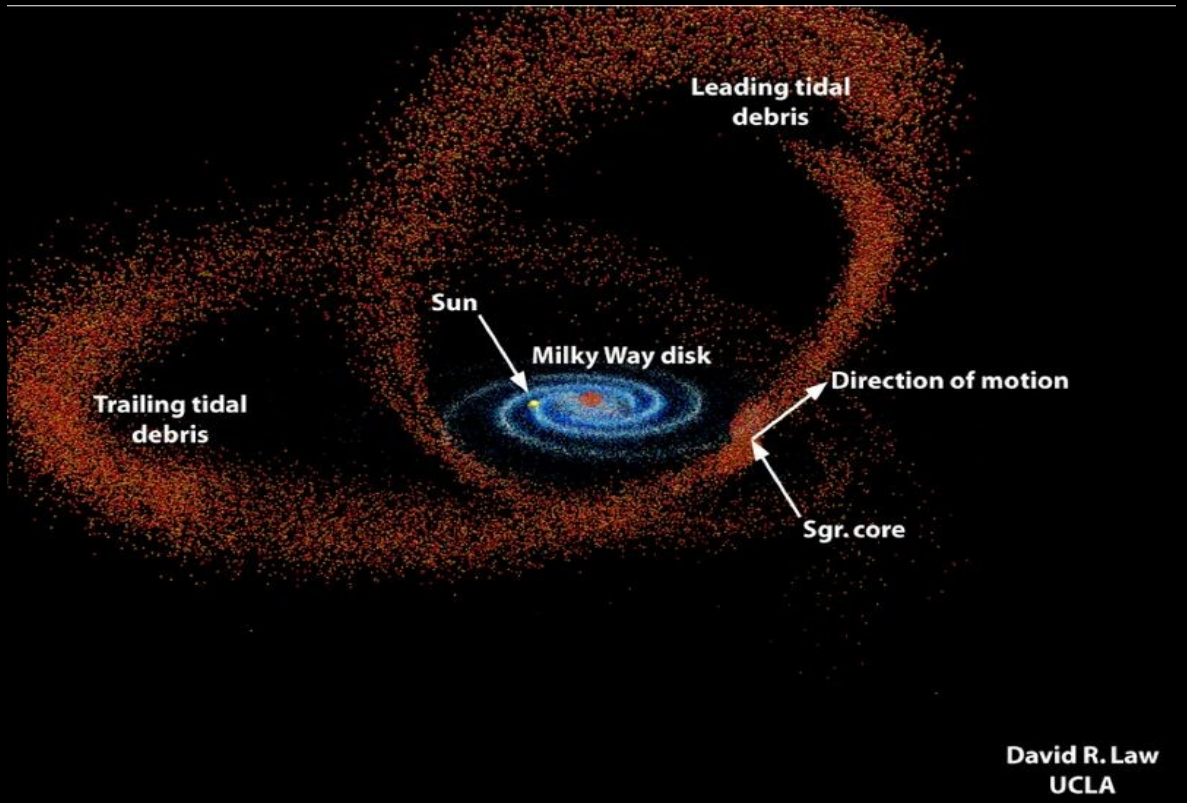

Sagittarius Stream

Stellar population

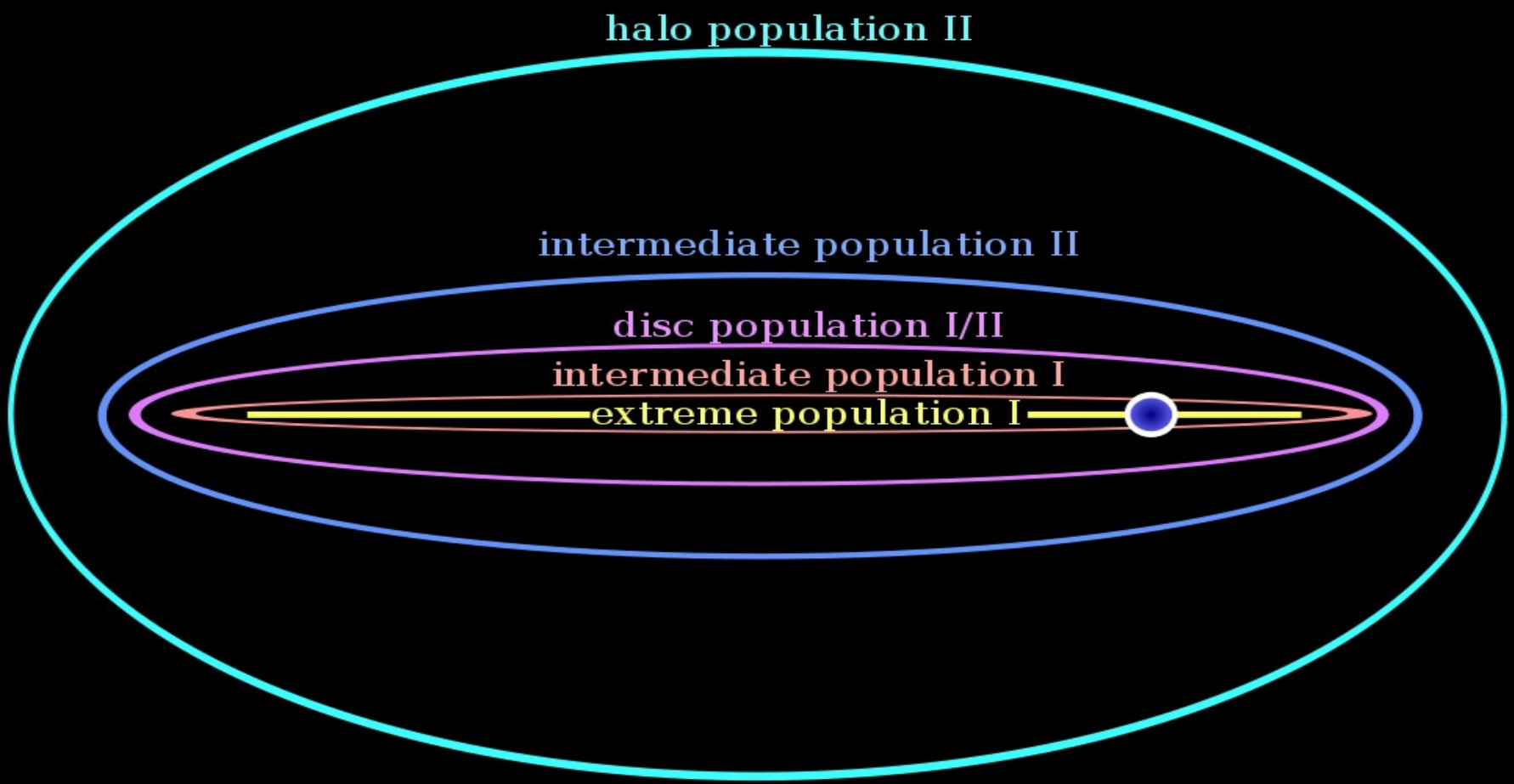

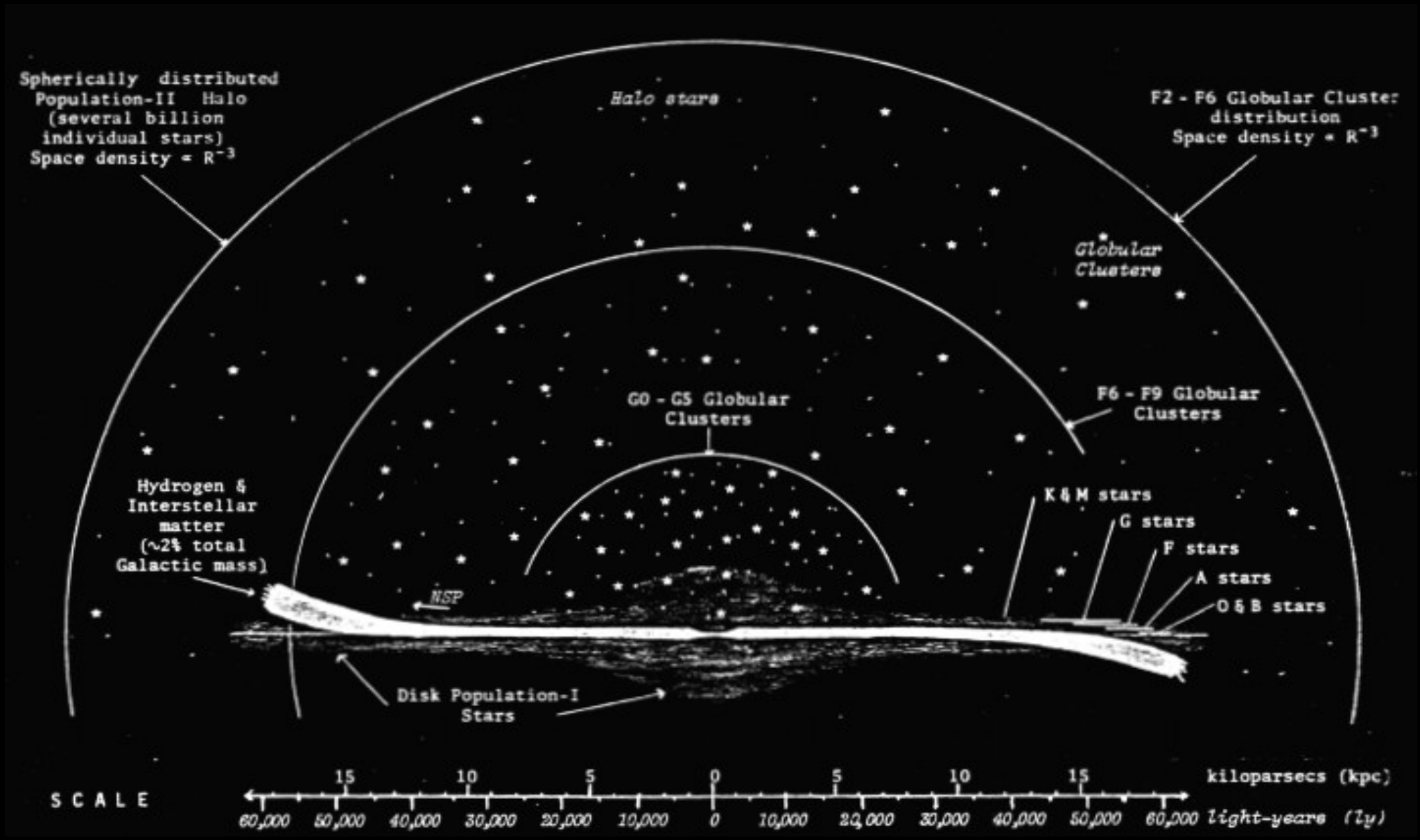
Spherically distributed Population-II Halo (several billion individual stars) Space density ∝ R^{-3}
Halo stars
F2 - F6 Globular Cluster distribution Space density ∝ R^{-3}
Globular Clusters
G0 - G5 Globular Clusters
F6 - F9 Globular Clusters
Hydrogen & Interstellar matter (~2% total Galactic mass)
K & M stars
G stars
F stars
A stars
O & B stars
NSP
Disk Population-I Stars
SCALE
15 10 5 0 5 10 15 kiloparsecs (kpc)
60,000 50,000 40,000 30,000 20,000 10,000 0 10,000 20,000 30,000 40,000 50,000 60,000 light-years (ly)

The Interstellar Medium

Interstellar Matter

- Molecular Clouds
- Neutral Hydrogen
- H II regions

Dust

InterStellar Radiation Field

- Stars,
- Dust
- CBM

Magnetic Field

Cosmic Rays

Energy density of the ISM

$$U_{ISRF} \sim 1\ \text{eV} / \text{cm}^3$$

$$U_{B} \sim 1\ \text{eV} / \text{cm}^3$$

$$E_{CR} \sim 1\ \text{eV} / \text{cm}^3$$

$$E_{gas} \sim 1\ \text{eV} / \text{cm}^3$$

Galactic Rotation Curve

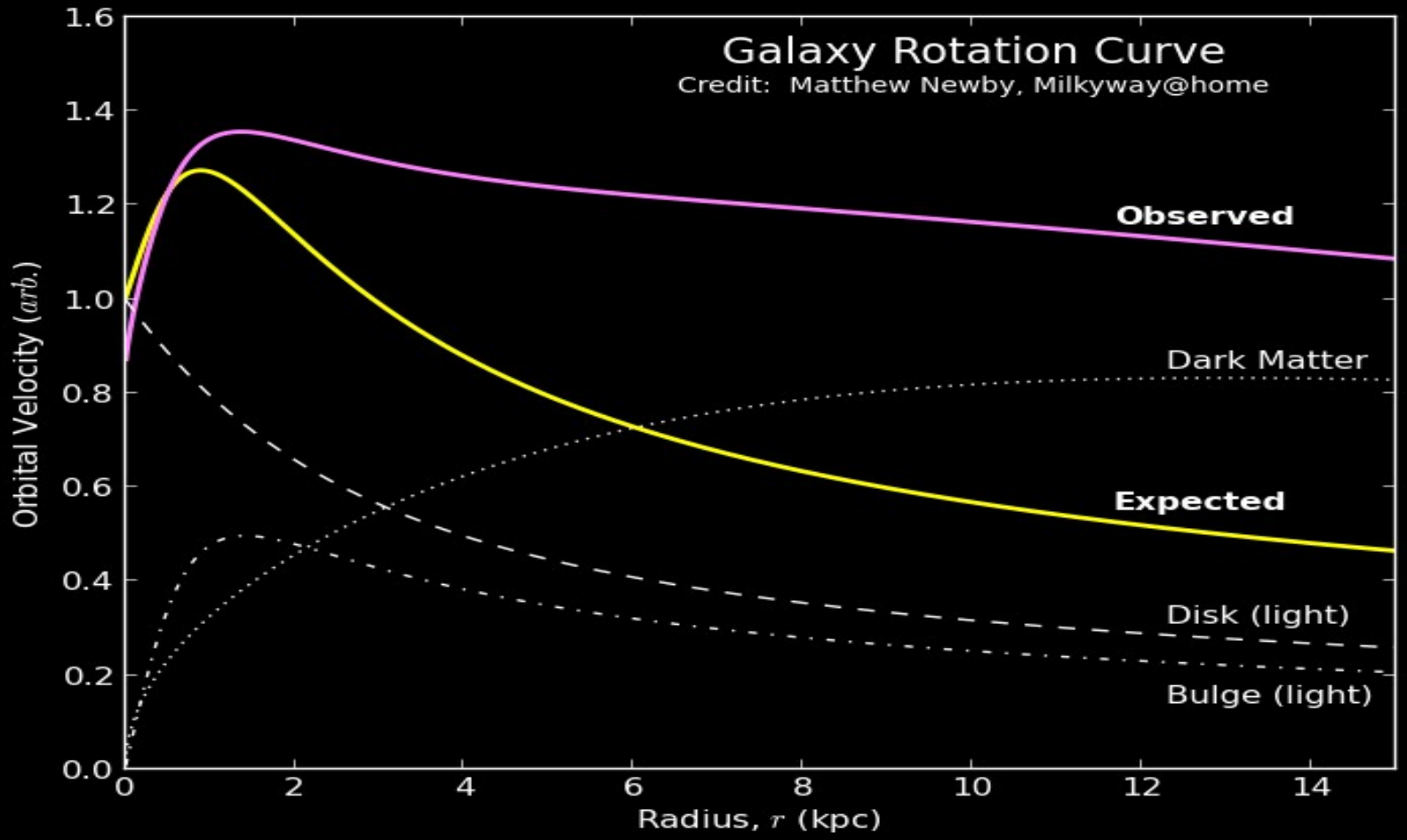

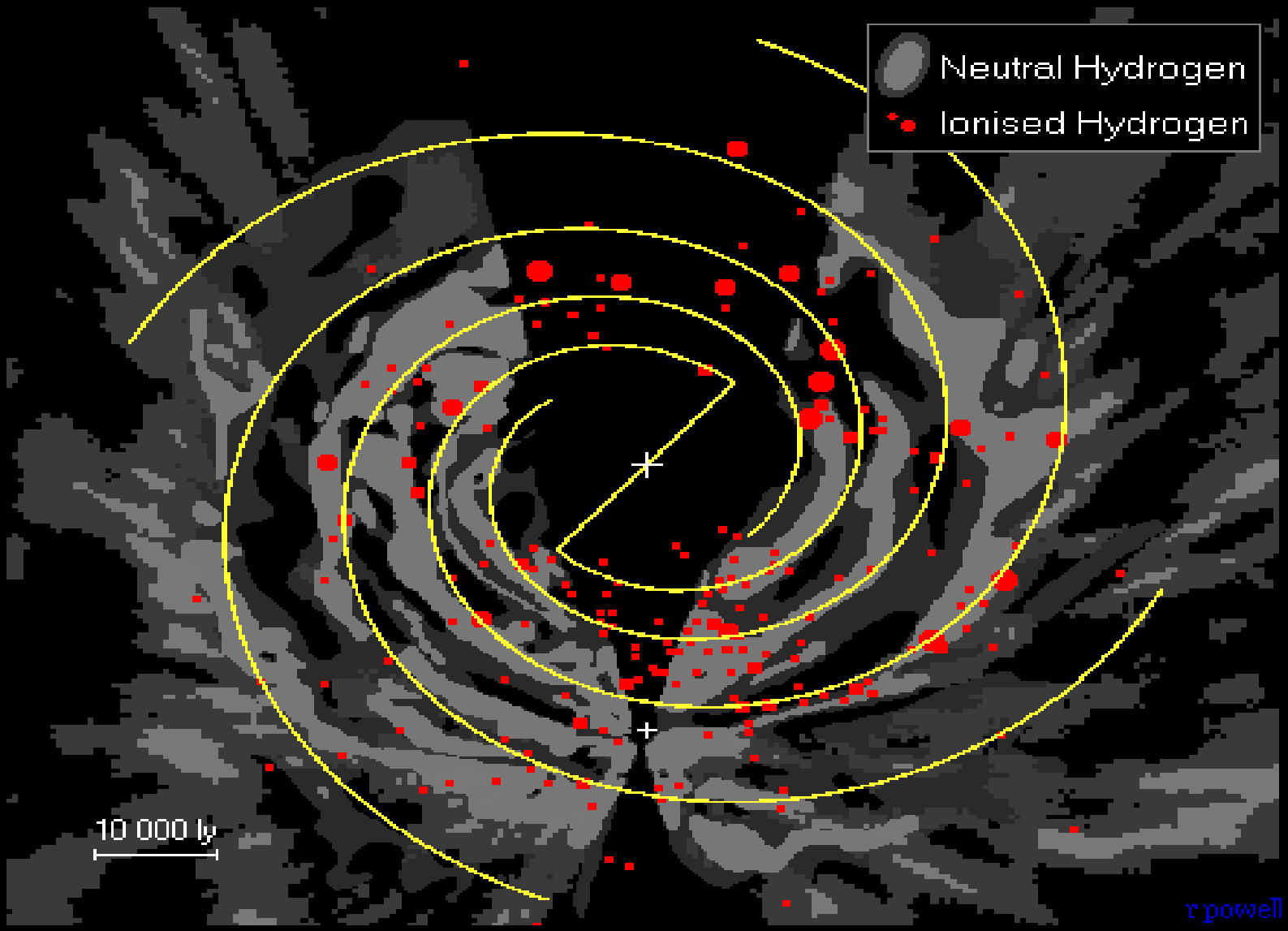
Neutral Hydrogen
Ionised Hydrogen
10 000 ly
r powell

Astronomy & Astrophysics manuscript no. ms
October 9, 2014

The observed spiral structure of the Milky Way⋆ ⋆⋆

L. G. Hou and J. L. Han

National Astronomical Observatories, Chinese Academy of Sciences, Jia-20, DaTun Road, ChaoYang District, 100012 Beijing, PR China
e-mail: lghou@nao.cas.cn, hjl@nao.cas.cn

Received 21 April 2014; accepted 7 July 2014

ABSTRACT

Context. The spiral structure of the Milky Way is not yet well determined. The keys to understanding this structure are to increase the number of reliable spiral tracers and to determine their distances as accurately as possible. HII regions, giant molecular clouds (GMCs), and 6.7 GHz methanol masers are closely related to high mass star formation, and hence they are excellent spiral tracers. The distances for many of them have been determined in the literature with trigonometric, photometric and/or kinematic methods.
Aims. We update the catalogs of Galactic HII regions, GMCs, and 6.7 GHz methanol masers, and then outline the spiral structure of the Milky Way.
Methods. We collected data for more than 2500 known HII regions, 1300 GMCs, and 900 6.7 GHz methanol masers. If the photometric or trigonometric distance was not yet available, we determined the kinematic distance using a Galaxy rotation curve with the current IAU standard, $R_0 = 8.5$ kpc and $\Theta_0 = 220$ km s^{-1}, and the most recent updated values of $R_0 = 8.3$ kpc and $\Theta_0 = 239$ km s^{-1}, after velocities of tracers are modified with the adopted solar motions. With the weight factors based on the excitation parameters of HII regions or the masses of GMCs, we get the distributions of these spiral tracers.
Results. The distribution of tracers shows at least four segments of arms in the first Galactic quadrant, and three segments in the fourth quadrant. The Perseus Arm and the Local Arm are also delineated by many bright HII regions. The arm segments traced by massive star forming regions and GMCs are able to match the HI arms in the outer Galaxy. We found that the models of three-arm and four-arm logarithmic spirals are able to connect most spiral tracers. A model of polynomial-logarithmic spirals is also proposed, which not only delineates the tracer distribution, but also matches the observed tangential directions.

Key words. Galaxy: disk – Galaxy: structure – Galaxy: kinematics and dynamics – HII regions – ISM: clouds

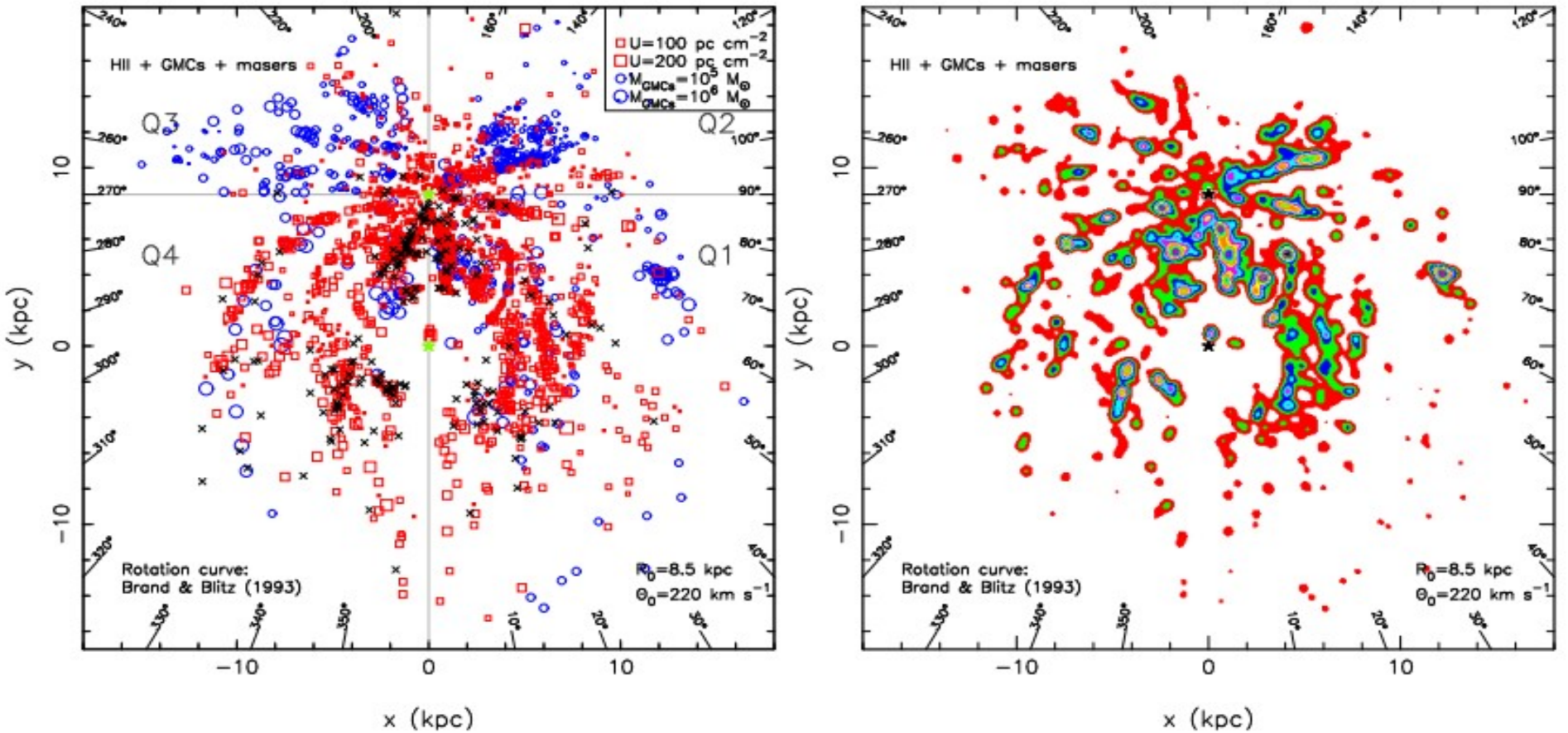

Fig. 15. *Left*: distributions of HII regions, GMCs, and 6.7 GHz methanol masers projected into the Galactic plane. The symbols are the same as those in Fig. 2. The kinematic distances are estimated using the rotation curve of BB93. *Right*: color intensity map of spiral tracers. The IAU standard R_0 = 8.5 kpc and Θ_0 = 220 km s^{-1} and standard solar motions are adopted in deriving the kinematic distances if no photometric or trigonometric distance is available.

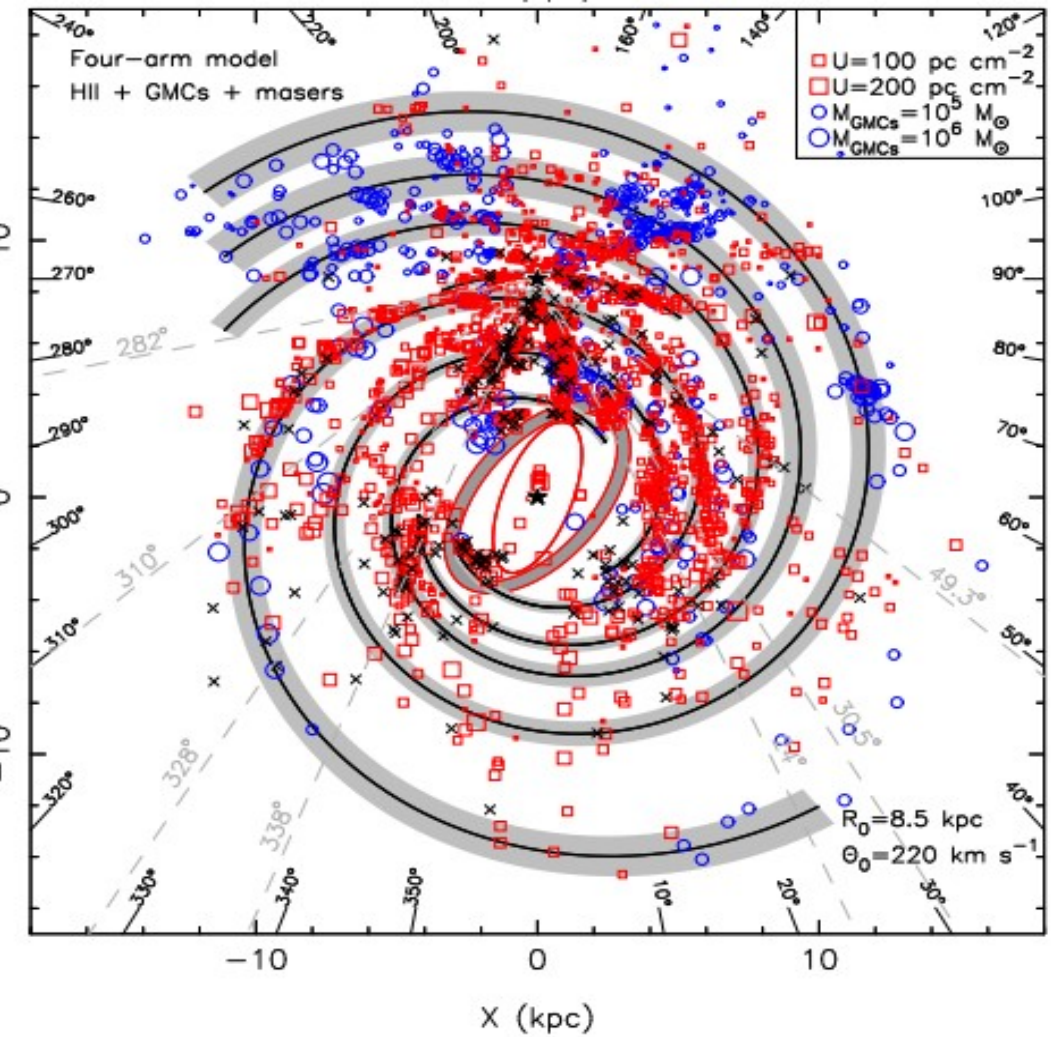

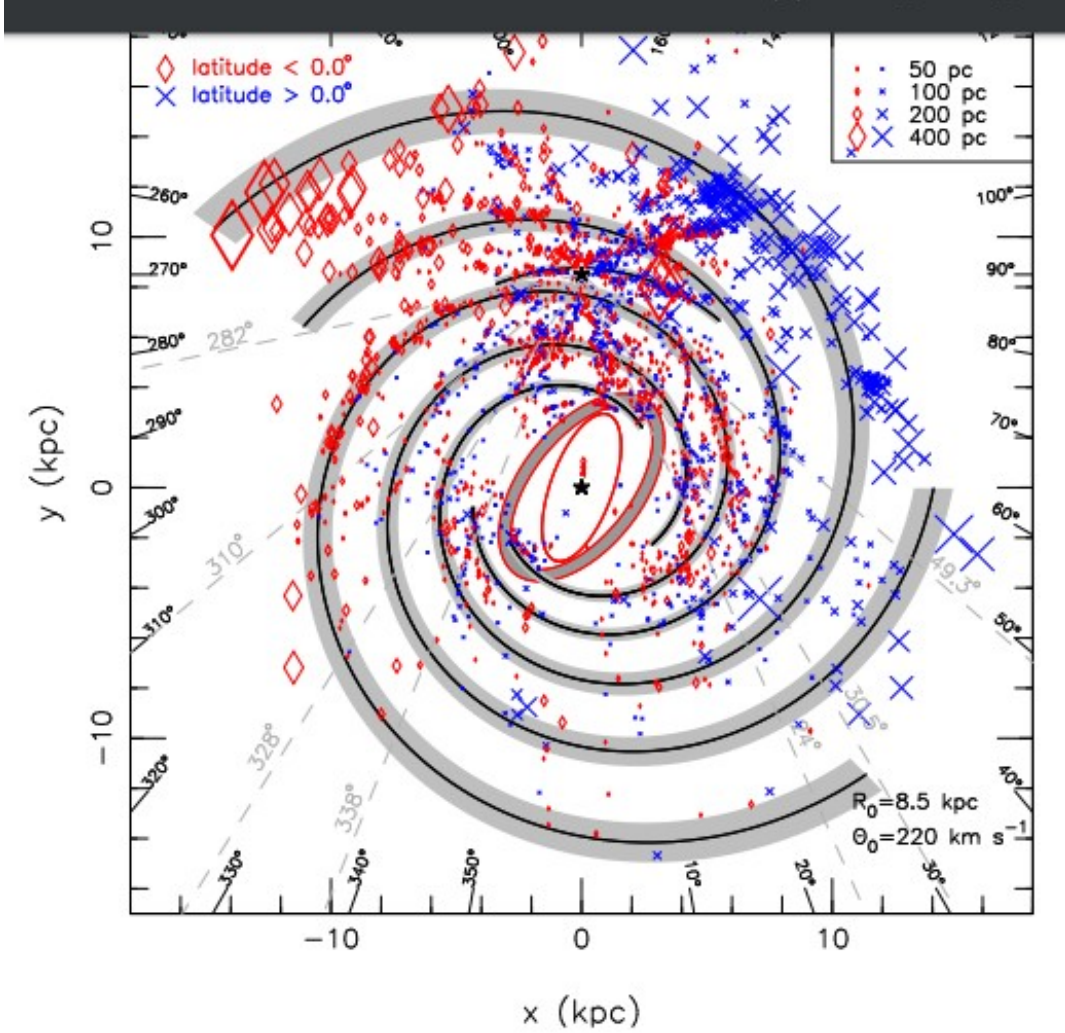

In polar coordinates (r, θ), the ith arm can be given as logarithmic form:

$$\ln \frac{r}{R_i} = (\theta - \theta_i) \tan \psi_i, \quad (3)$$

Fig. 16. Evidence of Galactic warp as shown by the distributions of HII regions, GMCs, and 6.7 GHz methanol masers. Note that the diamonds here indicate the tracers of $b < 0.0°$, and the blue crosses indicate the tracers of $b > 0.0°$. The symbol size is proportional to the offset from the Galactic plane. The outlines are the best-fitted four-arm model (see the *upper right panel* of Fig. 10).

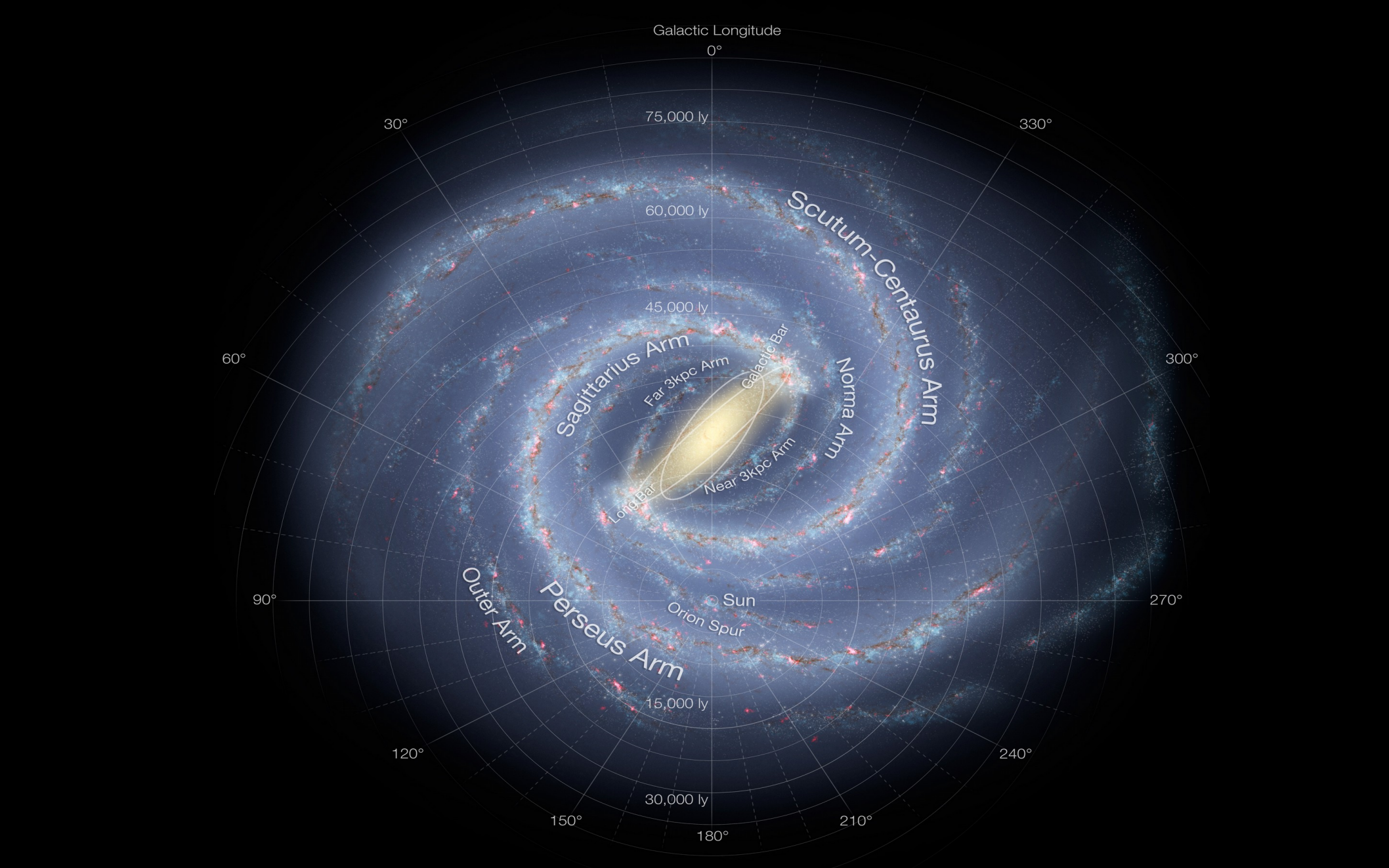
Galactic Longitude
0°
30°
330°
75,000 ly
60,000 ly
45,000 ly
60°
300°
Scutum-Centaurus Arm
Sagittarius Arm
Far 3kpc Arm
Galactic Bar
Norma Arm
Near 3kpc Arm
Long Bar
90°
270°
Outer Arm
Perseus Arm
Sun
Orion Spur
15,000 ly
120°
240°
30,000 ly
150°
210°
180°

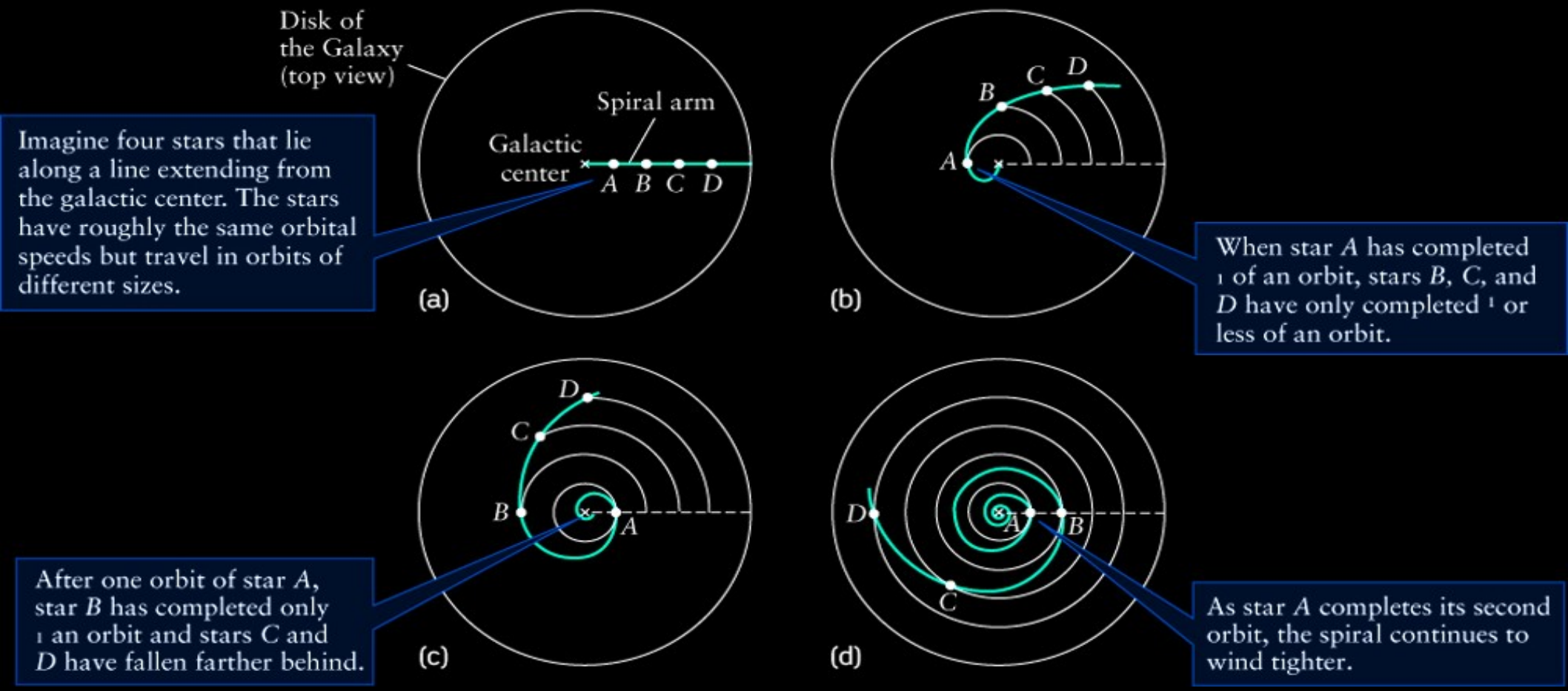
Disk of the Galaxy (top view)
Spiral arm
Galactic center
A B C D
(a)
Imagine four stars that lie along a line extending from the galactic center. The stars have roughly the same orbital speeds but travel in orbits of different sizes.
B C D
A
(b)
When star A has completed 1 of an orbit, stars B, C, and D have only completed 1 or less of an orbit.
D C B A
(c)
After one orbit of star A, star B has completed only 1 an orbit and stars C and D have fallen farther behind.
D A B C
(d)
As star A completes its second orbit, the spiral continues to wind tighter.

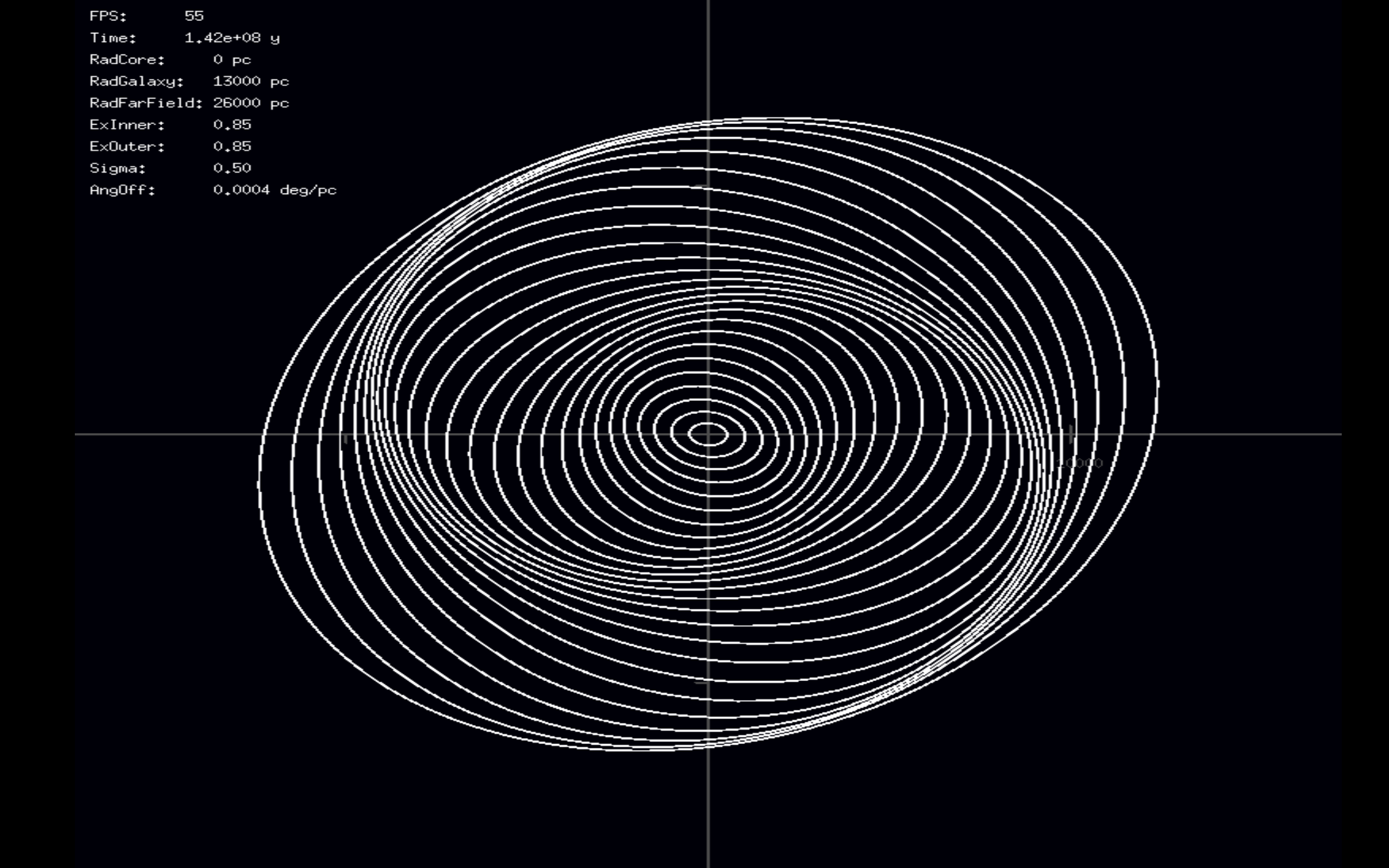
FPS: 55
Time: 1.42e+08 y
RadCore: 0 pc
RadGalaxy: 13000 pc
RadFarField: 26000 pc
ExInner: 0.85
ExOuter: 0.85
Sigma: 0.50
AngOff: 0.0004 deg/pc

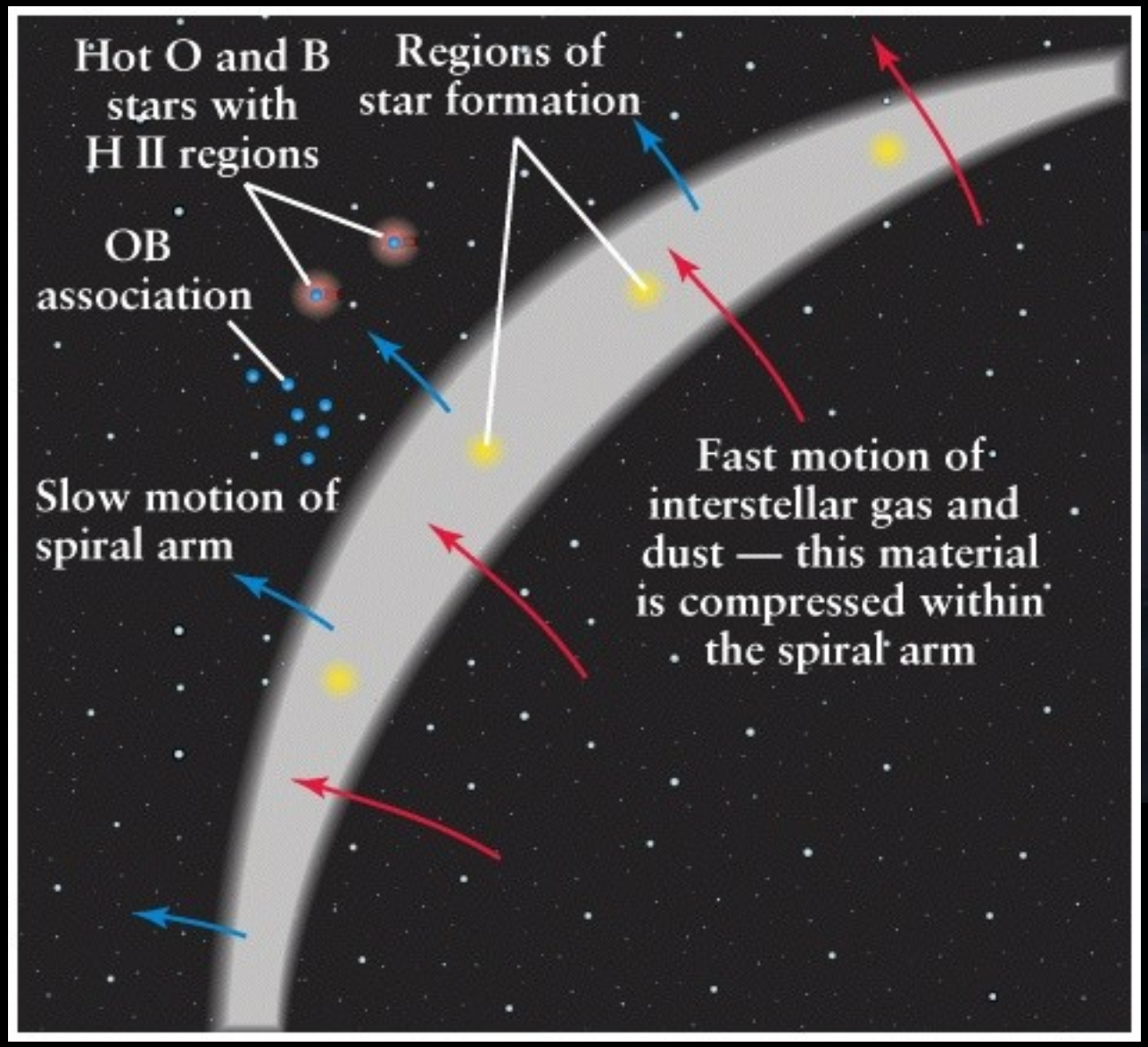
Hot O and B stars with H II regions
Regions of star formation
OB association
Slow motion of spiral arm
Fast motion of interstellar gas and dust — this material is compressed within the spiral arm

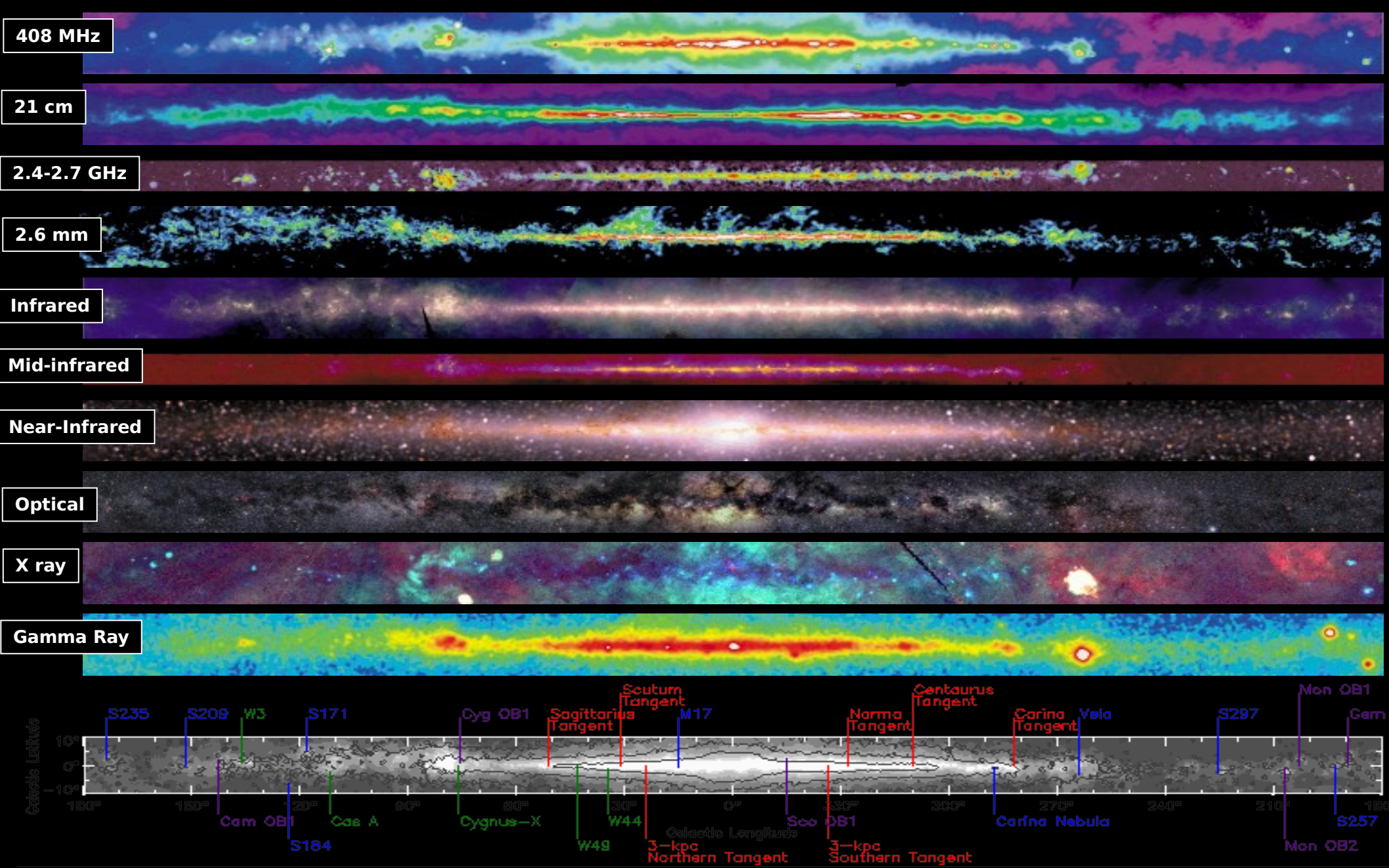
408 MHz
21 cm
2.4-2.7 GHz
2.6 mm
Infrared
Mid-infrared
Near-Infrared
Optical
X ray
Gamma Ray
S235
S209
W3
S171
Cyg OB1
Sagittarius Tangent
Scutum Tangent
M17
Norma Tangent
Centaurus Tangent
Carina Tangent
Vela
S297
Mon OB1
Gem
Cam OB1
S184
Cas A
Cygnus–X
W49
W44
3–kpc Northern Tangent
Sco OB1
3–kpc Southern Tangent
Carina Nebula
Mon OB2
S257
Galactic Latitude
Galactic Longitude

Radio Continuum (408 MHz)

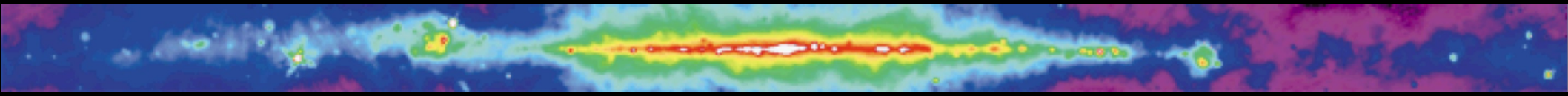

Intensity of radio continuum emission from high-energy charged particles in the Milky Way,from surveys with ground-based radio telescopes (Jodrell Bank Mark I and Mark IA, Bonn 100-meter, and Parkes 64-meter).

At this frequency, most of the emission is from electrons moving through the interstellar magnetic field at nearly the speed of light.

Shock waves from supernova explosions accelerate electrons to such high speeds, producing especially intense radiation near these sources.

Emission from the supernova remnant Cas A near 110° longitude is so intense that the diffraction pattern of the support legs for the radio receiver on the telescope is visible as a cross shape.

Atomic Hydrogen (1.4 GHz)

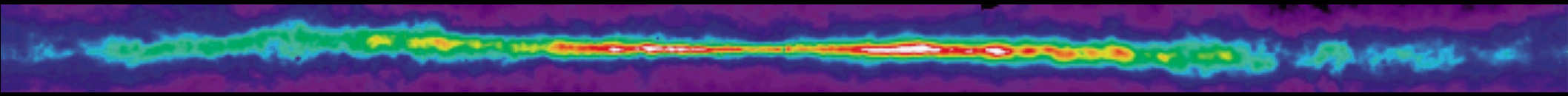

Column density of atomic hydrogen,derived on the assumption of optically thin emission, from radio surveys of the 21-cm transition of hydrogen.

The 21-cm emission traces the "cold and warm" interstellar medium, which on a large scale is organized into diffuse clouds of gas and dust that have sizes of up to hundreds of light-years.

Most of the image is based on the Leiden-Dwingeloo Survey of Galactic Neutral Hydrogen using the Dwingeloo 25-m radio telescope; the data were corrected for sidelobe contamination in collaboration with the University of Bonn.

Molecular Hydrogen (115 GHz)

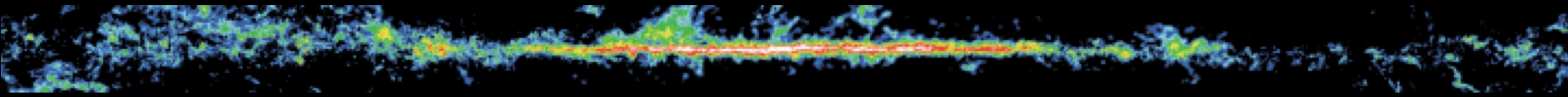

Column density of molecular hydrogen inferred from the intensity of the J =1-0 spectral line of carbon monoxide, a standard tracer of the cold, dense parts of the interstellar medium.

Such gas is concentrated in the spiral arms in discrete "molecular clouds."

Most molecular clouds are sites of star formation.

The molecular gas is pre-dominantly H_2, but H_2 is difficult to detect directly at interstellar conditions and CO, the second most abundant molecule, is observed as a surrogate.

The column densities were derived on the assumption of a constant proportionality between the column density of H_2 and the intensity of the CO emission.

Infrared (12–100 microns)

Composite mid-and far-infrared intensity observed by the Infrared Astronomical Satellite (IRAS) in 12, 60, and 100 micron wavelength bands.

The images are encoded in the blue, green, and red color ranges, respectively.

Most of the emission is thermal, from interstellar dust warmed by absorbed starlight, including star-forming regions embedded in interstellar clouds.

The display here is a mosaic of IRAS Sky Survey Atlas images.

Emission from interplanetary dust in the solar system, the "zodiacal emission," was modeled and subtracted in the production of the Atlas.

Radio Continuum (2.4 - 2.7 GHz)

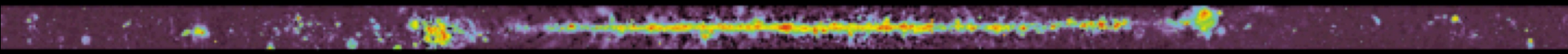

Intensity of radio continuum emission from hot, ionized gas and high-energy electrons in the Milky Way, from surveys with both the Bonn 100-meter, and Parkes 64-meter radio telescopes.

Unlike most other views of our Galaxy presented here, these data extend to latitudes of only 5° from the Galactic plane.

The majority of the bright emission seen in the image is from hot, ionized regions, or is produced by energetic electrons moving in magnetic fields.

The higher resolution of this image, relative to the 408 MHz picture above, shows Galactic objects in more detail.

Note that the bright "ridge" of Galactic radio emission, appearing prominently in the 408 MHz image, has been subtracted here in order to show Galactic features and objects more clearly.

Mid-Infrared

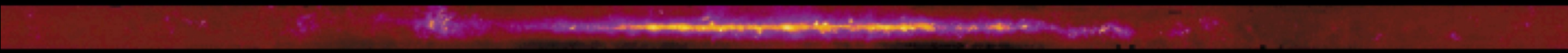

Mid-infrared emission observed by the SPIRIT III instrument on the Midcourse Space Experiment (MSX) satellite.

Most of the diffuse emission in this wavelength band is believed to come from complex molecules called polycyclic aromatic hydrocarbons, which are commonly found both in coal and interstellar gas clouds.

Red giant stars, planetary nebulae, and massive stars so young that they remain deeply embedded in their parental molecular gas clouds produce the multitude of small bright spots seen here.

Unlike most of the other maps, this map extends only to 5° above and below the Galactic plane.

Near Infrared (1.25-3.5 microns)

Composite near-infrared intensity observed by the Diffuse Infrared Background Experiment (DIRBE) instrument on the Cosmic Background Explorer (COBE) in the 1.25, 2.2, and 3.5 micron wavelength bands.

The images are encoded in the blue, green, and red color ranges, respectively.

Most of the emission at these wavelengths is from relatively cool giant K stars in the disk and bulge of the Milky Way. Interstellar dust does not strongly obscure emission at these wavelengths; the maps trace emission all the way through the Galaxy, although absorption in the 1.25 micron band is evident toward the Galactic center region.

Optical (400-600 nm)

Due to the strong obscuring effect of interstellar dust,the light is primarily from stars within a few thousand light-years of the Sun, nearby on the scale of the Milky Way.

The widespread bright red regions are produced by glowing, low-density gas.

Dark patches are due to absorbing clouds of gas and dust.

Stars differ from one another in color, as well as mass, size and luminosity. Interstellar dust scatters blue light preferentially, reddening the starlight somewhat relative to its true color and producing a diffuse bluish glow. This scattering, as well as absorption of some of the light by dust, also leaves the light diminished in brightness.

The panorama was assembled from sixteen wide-angle photographs taken by Dr. Axel Mellinger using a standard 35-mm camera and color negative film. The exposures were made between July 1997 and January 1999 at sites in the United States, South Africa, and Germany.

X Rays (0.25-1.5 keV)

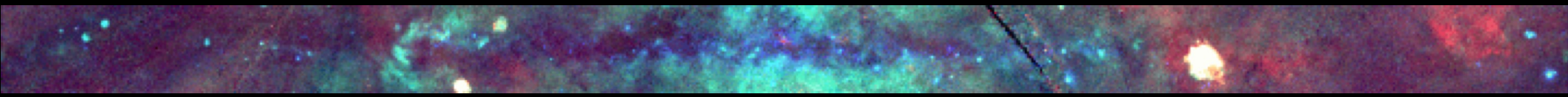

Composite X-ray intensity observed by the Position-Sensitive Proportional Counter (PSPC) instrument on the Röntgen Satellite (ROSAT).

Images in three broad, soft X-ray bands centered at 0.25 , 0.75, and 1.5 keV are encoded in the red, green, and blue color ranges, respectively.

In the Milky Way, extended soft X-ray emission is detected from hot, shocked gas.

At the lower energies especially, the interstellar medium strongly absorbs X-rays, and cold clouds of interstellar gas are seen as shadows against background X-ray emission.

Color variations indicate variations of absorption or of the temperatures of the emitting regions. The black regions indicate gaps in the ROSAT survey.

Gamma Rays (E>300 MeV)

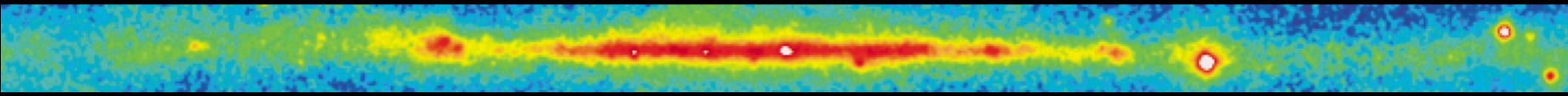

Intensity of high-energy gamma-ray emission observed by the Energetic Gamma-Ray Experiment Telescope (EGRET) instrument on the Compton Gamma-Ray Observatory (CGRO).

The image includes all photons with energies greater than 300 MeV. At these extreme energies, most of the celestial gamma rays originate in collisions of cosmic rays with hydrogen nuclei in interstellar clouds.

The bright, compact sources near Galactic longitudes 185°, 195°, and 265° indicate high-energy phenomena associated with the Crab, Geminga, and Vela pulsars, respectively.